The REBELS ALMA Survey: efficient Ly α transmission of UV-bright $z \simeq$ 7 galaxies from large velocity offsets and broad line widths

Ryan Endsley [iD],[1]★ Daniel P. Stark,[1] Rychard J. Bouwens,[2] Sander Schouws,[2] Renske Smit,[3]
Mauro Stefanon [iD],[2] Hanae Inami [iD],[4] Rebecca A. A. Bowler [iD],[5,6] Pascal Oesch,[7,8] Valentino Gonzalez,[9,10]
Manuel Aravena,[11] Elisabete da Cunha,[12] Pratika Dayal [iD],[13] Andrea Ferrara,[14] Luca Graziani [iD],[15,16]
Themiya Nanayakkara [iD],[17] Andrea Pallottini [iD],[14] Raffaella Schneider [iD],[15,18,19,20] Laura Sommovigo [iD],[14]
Michael Topping,[1] Paul van der Werf[2] and Anne Hutter [iD][13]

Affiliations are listed at the end of the paper

ABSTRACT

Recent work has shown that UV-luminous reionization-era galaxies often exhibit strong Lyman-alpha emission despite being situated at redshifts where the IGM is thought to be substantially neutral. It has been argued that this enhanced Ly α transmission reflects the presence of massive galaxies in overdense regions which power large ionized bubbles. An alternative explanation is that massive galaxies shift more of their Ly α profile to large velocities (relative to the systemic redshift) where the IGM damping wing absorption is reduced. Such a mass-dependent trend is seen at lower redshifts, but whether one exists at $z \sim 7$ remains unclear owing to the small number of existing systemic redshift measurements in the reionization era. This is now changing with the emergence of [C II]-based redshifts from ALMA. Here, we report MMT/Binospec Ly α spectroscopy of eight UV-bright ($M_{UV} \sim -22$) galaxies at $z \simeq 7$ selected from the ALMA REBELS survey. We detect Ly α in four of eight galaxies and use the [C II] systemic redshifts to investigate the Ly α velocity profiles. The Ly α lines are significantly redshifted from systemic (average velocity offset $= 223 \, \mathrm{km \, s^{-1}}$) and broad (FWHM ≈ 300–$650 \, \mathrm{km \, s^{-1}}$), with two sources showing emission extending to $\approx 750 \, \mathrm{km \, s^{-1}}$. We find that the broadest Ly α profiles are associated with the largest [C II] line widths, suggesting a potential link between the Ly α FWHM and the dynamical mass. Since Ly α photons at high velocities transmit efficiently through the $z = 7$ IGM, our data suggest that velocity profiles play a significant role in boosting the Ly α visibility of the most UV-luminous reionization-era galaxies.

Key words: galaxies: evolution – galaxies: high-redshift – dark ages, reionization, first stars.

1 INTRODUCTION

Reionization is a landmark event of early cosmic history, reflecting when the first luminous objects began ionizing nearly every hydrogen atom in the Universe (Dayal & Ferrara 2018; Robertson 2022). Over the past decade, substantial progress has been made in revealing the timeline of reionization thanks to a variety of observational efforts. The frequent detections of Ly α and Ly β forests in the spectra of $z \sim 6$ quasars indicate that reionization was largely complete by $z = 5.9$ with an IGM neutral fraction $x_{HI} \lesssim 10$ per cent (McGreer, Mesinger & D'Odorico 2015). Quasars at slightly higher redshifts ($z = 7 - 7.5$) show strong Lyman-alpha damping wing features, indicating a significantly neutral IGM only $\approx 200 \, \mathrm{Myr}$ earlier ($x_{HI} \sim 50$ per cent; Mortlock et al. 2011; Greig et al. 2017; Bañados et al. 2018; Davies et al. 2018; Wang et al. 2020; Yang et al. 2020). This timeline is consistent with the reionization mid-point of $z = 7.8 \pm 0.7$ inferred from the cosmic microwave background (CMB; Planck Collaboration VI 2020).

Lyman-alpha emission from high-redshift galaxies is another tool often utilized to study reionization (Ouchi, Ono & Shibuya 2020). Because Ly α resonantly interacts with H I, its observed strength is very sensitive to the ionization state of the surrounding IGM (e.g. Miralda-Escudé 1998). Deep spectroscopic surveys have demonstrated that the fraction of typical star-forming galaxies showing strong (rest-frame equivalent width > 25 Å) Ly α emission declines abruptly at $z > 6$ (Fontana et al. 2010; Stark et al. 2010; Ono et al. 2012; Caruana et al. 2014; Pentericci et al. 2014, 2018; Schenker et al. 2014; Jung et al. 2017, 2020; Hoag et al. 2019; Fuller et al. 2020) suggesting a highly neutral IGM at $z \sim 7$–7.5 ($x_{HI} \gtrsim 50$ per cent; e.g. Mason et al. 2018a; Hoag et al. 2019; Jung et al. 2020; Whitler et al. 2020). It has also been shown that the faint end of the Ly α luminosity function declines faster than the UV continuum luminosity function at $z > 6$ (Hu et al. 2010; Ouchi et al. 2010; Kashikawa et al. 2011; Konno et al. 2014, 2018; Ota et al. 2017; Zheng et al. 2017; Itoh et al. 2018; Hu et al. 2019; cf. Wold et al. 2022), suggesting a similar reionization timeline consistent with inferences from quasars and the CMB.

Over the past few years, attention has shifted towards using Ly α observations to study the structure of reionization. Recent data suggest that the Ly α emission strengths of UV-bright ($M_{UV} \lesssim -21$)

galaxies do not strongly evolve between $z \sim 6$ and $z \sim 7$ (Stark et al. 2017; Endsley et al. 2021b), even though the neutrality of the IGM changes substantially over this time period. One likely explanation for these findings is that UV-bright galaxies (which preferentially trace massive systems; e.g. Barone-Nugent et al. 2014; Harikane et al. 2018a) often reside in large ionized bubbles powered by the enhanced number of neighbouring galaxies in their local overdensities (e.g. Wyithe & Loeb 2005; Dayal et al. 2009; Zitrin et al. 2015; Castellano et al. 2016; Hutter et al. 2017; Weinberger et al. 2018; Endsley et al. 2021b; Garaldi et al. 2022; Kannan et al. 2022; Leonova et al. 2022; Qin et al. 2022). The presence of these H II regions boosts Ly α transmission by enabling the photons to cosmologically redshift past the resonant core and into the damping wing before encountering intergalactic H I (Mesinger, Haiman & Cen 2004; Mason & Gronke 2020; Park et al. 2021; Smith et al. 2022). Reports of UV-bright Ly α-emitting galaxies at $z \gtrsim 7$ lying in close proximity may further support the picture that large ionized structures commonly surrounded early massive galaxies (Vanzella et al. 2011; Castellano et al. 2018; Jung et al. 2020; Tilvi et al. 2020; Hu et al. 2021; Endsley et al. 2021b; Endsley & Stark 2022).

However, ionized bubbles are not the only mechanism capable of boosting Ly α transmission during reionization. Resonant interactions within galaxies can shift Ly α emission redward of systemic velocity by $\gtrsim 100 \, \text{km s}^{-1}$ (e.g. Shapley et al. 2003; Erb et al. 2014; Shibuya et al. 2014), and thereby push the photons into the damping wing even before they escape the CGM. If such high Ly α velocity offsets are common among luminous reionization-era galaxies, this would help explain their enhanced Ly α visibility and lessen the need for very large H II regions in their vicinity (e.g. Stark et al. 2017; Mason et al. 2018b). Unfortunately, our understanding of velocity offsets at $z > 6$ has remained limited by challenges in detecting not only Ly α from such early systems, but also a non-resonant line tracing the systemic redshift (e.g. [C II]158 μm). As a result, there are currently only four Ly α velocity offset measurements among extremely UV-luminous ($M_{\text{UV}} < -22$) Lyman-break selected galaxies at $z > 6$ (Willott et al. 2015; Stark et al. 2017; Hashimoto et al. 2019). Until a better census of these velocity offsets is obtained, considerable uncertainties will persist in how to connect the Ly α transmission of $z \gtrsim 7$ galaxies to the structure of reionization.

In this work, we aim to significantly increase the number of Ly α velocity offset measurements among UV-luminous reionization-era galaxies. Recently, the ongoing ALMA large program REBELS (Reionization-Era Bright Emission Line Survey; Bouwens et al. 2022) yielded systemic [C II]158- μm line detections from ≥22 UV-bright ($-23 \lesssim M_{\text{UV}} \lesssim -21.5$) galaxies at $z \geq 6.5$ (Schouws et al., in preparation). Using the optical MMT/Binospec spectrograph, we have obtained Ly α spectra of a substantial fraction (50 per cent; 8/16) of [C II]-detected REBELS galaxies in the redshift range $z = 6.5$–7.1. With this combined UV + IR data set, we explore the role of velocity offsets on Ly α IGM transmission among UV-luminous $z \simeq 7$ galaxies. Our data additionally reveal how the broad Ly α line widths of these systems impact transmission through a partially neutral IGM.

This paper is organized as follows. In Section 2, we describe the sub-sample of $z \simeq 7$ REBELS galaxies which we have thus far targeted with MMT/Binospec, as well as the details of those spectroscopic observations. We present the Ly α spectra in Section 3, commenting on the resulting emission line strengths and line widths. We then utilize our ALMA [C II] detections to place the Binospec spectra into the systemic reference frame and measure Ly α velocity offsets (Section 4.1). In Section 4.2, we discuss the broad Ly α lines seen among our galaxies. We then test whether our sample shows

Table 1. Summary of our MMT/Binospec observations. REBELS-14 and REBELS-39 were each observed with two separate masks and we provide details for each mask.

ID	Exposure Time (s)	Seeing (arcsec)	Wavelength Coverage (Å)	PA (deg)
REBELS-03	13500	0.73	7385–9909	−37.0
REBELS-05	13500	0.73	6993–9516	− 37.0
REBELS-14	22500	0.87	7548–10070	− 52.0
	27000	0.91	7783–10306	− 12.0
REBELS-15	18900	0.91	7806–10330	− 116.2
REBELS-23	23400	0.99	7435–9959	− 98.5
REBELS-26	32400	1.09	7207–9731	− 98.5
REBELS-27	16200	0.94	7493–10017	− 98.5
REBELS-39	7200	0.98	7250–9773	+ 45.0
	14400	0.73	7355–9875	− 155.0

any evidence of a connection between [C II] luminosity at fixed SFR and Ly α equivalent width (Section 4.3). Finally, we discuss how the large velocity offsets and broad line widths of massive, UV-luminous reionization-era galaxies result in efficient Ly α transmission through a significantly neutral IGM (Section 5). We summarize our main conclusions in Section 6.

In this work, we quote all magnitudes in the AB system, assume a Chabrier (2003) initial mass function (IMF) with limits of 0.1–$300 \, M_{\odot}$, and adopt a flat ΛCDM cosmology with parameters $h = 0.7$, $\Omega_{\text{M}} = 0.3$, and $\Omega_{\Lambda} = 0.7$.

2 DATA

In this work, we focus on a sample of $z \simeq 7$ galaxies with recent [C II] detections from the ALMA large program REBELS (Fudamoto et al. 2021; Bouwens et al. 2022). REBELS (still ongoing) is targeting 40 UV-bright ($-23 \lesssim M_{\text{UV}} \lesssim -21.5$) Lyman-break selected galaxies at $z \geq 6.5$. These systems were primarily selected from the wide-area COSMOS and XMM fields ($\sim 7 \, \text{deg}^2$ total). Here, we use the Cycle 7 data from REBELS which delivered the large majority (~ 85 per cent) of all planned observations for this program. The details of the ALMA data reduction and processing for [C II] and dust continuum are described in Schouws et al. (in preparation) and Inami et al. (2022), respectively. In this section, we begin by describing our spectroscopic Ly α observations for a subset of these REBELS galaxies (Section 2.1) and then detail how we infer physical properties among our Ly α-targeted sample (Section 2.2).

2.1 Lyman-alpha observations

We have thus far targeted Ly α emission in eight [C II]-detected REBELS galaxies at $z = 6.5$–7.1 using the MMT/Binospec optical spectrograph (Fabricant et al. 2019). For all observations, we utilized the 600 l mm^{-1} grating which provides sensitive coverage between ≈ 0.7 and 1 μm at moderate resolution ($R \approx 4400$) given our adopted slit width of 1.0 arcsec. We report the total exposure time, average seeing, wavelength coverage, and mask position angle (PA) describing the Binospec observations of each REBELS source in Table 1. The typical exposure time per source was 5.6 h with a typical seeing of 0.9 arcsec. Two of our target REBELS galaxies (REBELS-14 and REBELS-39) were observed using two separate masks with slightly different wavelength coverage and PA (see Table 1). Initial Ly α results of REBELS-14, REBELS-15, REBELS-23, REBELS-26, and REBELS-39 were previously presented in Endsley et al. (2021b, hereafter E21b) and therein identified as

XMM3-227436, XMM3-504799, COS-469110, COS-534584, and COS-862541, respectively. Here, we extend this previous work by exploring the Ly α emission properties of this sample in greater detail using the [C II] and dust continuum information now available from our ALMA observations. Furthermore, we have since obtained significantly deeper (i.e. 3–5 × longer exposure time) Binospec data on REBELS-14 and REBELS-39 enabling a more detailed analysis of their Ly α line profiles.

Our Binospec data reduction largely follows the approach described in E21b, which we briefly review here. We first process each individual exposure separately using the public Binospec data reduction pipeline (Kansky et al. 2019) which performs telluric correction. We then coadd each exposure (for an individual mask) using the weighting scheme of Kriek et al. (2015) and apply optimal extraction (Horne 1986) to obtain the 1D spectra of each source. To determine the spatial axis width for the optimal extraction, we first fit a Gaussian to the observed emission line profile. Absolute flux calibration is determined using the spectra of multiple bright stars placed on each mask. For REBELS-14 and REBELS-39, we coadd the data between different masks using an inverse variance weighting approach. Slit loss correction factors are derived by adopting the size–luminosity relation from Curtis-Lake et al. (2016) and assuming a Sérsic profile with $n = 1.0$, resulting in small correction factors of ≈5–10 per cent. Because these slit loss corrections assume that the Ly α surface brightness profile tracks the rest-UV emission, our reported fluxes will underestimate the total line flux throughout the extended Ly α halo surrounding each galaxy. We also compute the Ly α EWs following the approach of E21b as we aim to compare the EWs of our REBELS sources to the EW distribution inferred among UV-bright ($-22.5 \lesssim M_{UV} \lesssim -20.5$) $z \sim 7$ galaxies in E21b. That is, we adopt a continuum flux density (in μJy) from the photometric band closest to Ly α yet fully redward of the Ly α break, which effectively assumes a flat UV continuum (i.e. $\beta = -2$ where $F_\lambda \propto \lambda^{\beta + 2}$) between Ly α and the adopted band. While the true continuum is likely weaker immediately redward of Ly α (e.g. Shapley et al. 2003; Steidel et al. 2016), we use the photometric continuum approach above since high signal-to-noise ratio (S/N) spectroscopic UV continuum measurements do not yet exist for our galaxies.

For objects with no apparent Ly α detection, we determine upper limits on the Ly α EW by calculating the integrated noise from the fully reduced 1D spectrum over a wavelength interval assumed relevant for the Ly α line. This wavelength interval is set to begin at a value corresponding to the assumed Ly α redshift and spans a range equivalent to an assumed FWHM of the line. We assume a range of possible Ly α redshifts corresponding to velocity offsets of $\Delta v_{Ly\alpha} = 0$–$800\,\mathrm{km\,s^{-1}}$ relative to [C II], where these values encompass all robust $\Delta v_{Ly\alpha}$ measurements in the literature at $z > 6$ (see Table 4). Given the broad Ly α profiles observed in our four Ly α-detected REBELS sources (Section 3), we consider line widths ranging between FWHM = 300 and $700\,\mathrm{km\,s^{-1}}$. The range of 5σ upper limits for each REBELS galaxy not detected in Ly α is reported in Table 3, where these limits depend on not only the total exposure time and seeing of the observations, but also whether skylines are impacting the spectrum noise around the possible Ly α feature.

2.2 Galaxy properties

The physical properties (e.g. stellar mass and [O III] + H β EW) of each REBELS galaxy are inferred using the SED fitting code BEAGLE (Chevallard & Charlot 2016). BEAGLE adopts the photoionization models of star-forming galaxies from Gutkin, Charlot & Bruzual (2016) which incorporate both stellar and nebular emission by

Table 2. Summary of the galaxy properties inferred for each of REBELS source considered in this work. Absolute UV magnitudes are reported at rest-frame 1600 Å. The [O III] + H β EWs and stellar masses are inferred using the BEAGLE SED fitting code as described in Section 2.2. We note that these values differ from those in the fiducial REBELS catalogue (Stefanon et al., in preparation) due to our alternate SED fitting approach (see Section 2.2). The reported errors do not account for uncertainties in modelling assumptions (e.g. star formation history), though we briefly discuss such uncertainties in the text.

ID	M_{UV}	$\log(M_*/M_\odot)$	[O III] + H β EW (Å)
REBELS-03	-21.8 ± 0.3	$8.9^{+0.6}_{-0.6}$	510^{+650}_{-320}
REBELS-05	-21.6 ± 0.2	$8.9^{+0.7}_{-0.5}$	1060^{+920}_{-530}
REBELS-14	-22.7 ± 0.4	$8.7^{+0.4}_{-0.3}$	1520^{+1300}_{-900}
REBELS-15	-22.6 ± 0.3	$9.1^{+0.3}_{-0.2}$	4570^{+1830}_{-1940}
REBELS-23	-21.6 ± 0.5	$8.8^{+0.4}_{-0.5}$	830^{+520}_{-340}
REBELS-26	-21.8 ± 0.1	$9.1^{+0.5}_{-0.7}$	800^{+640}_{-390}
REBELS-27	-21.9 ± 0.2	$9.5^{+0.3}_{-1.0}$	310^{+340}_{-210}
REBELS-39	-22.7 ± 0.2	$8.7^{+0.3}_{-0.1}$	3250^{+1010}_{-930}

combining the latest version of the Bruzual & Charlot (2003) stellar population synthesis models with CLOUDY (Ferland et al. 2013). We assume a delayed star formation history (SFR $\propto te^{-t/\tau}$) with an allowed recent (<10 Myr) burst and we force star formation to have begun at least 1 Myr ago, consistent with the fitting approach of Endsley et al. (2021a) and E21b. While the fiducial REBELS SED fits assume a constant star formation history (Stefanon et al., in preparation), our motivation for adopting this alternative 'delayed + burst' fitting approach is twofold. First, we wish to provide a self-consistent comparison of [O III] + H β EWs with those inferred in Endsley et al. (2021a) since it has been shown that higher [O III] + H β EWs connect to larger Ly α EWs at $z \sim 7$ (Castellano et al. 2017, E21b). Secondly, we aim to open up the possibility that the subset of our sources with very strong IRAC colours (and hence very large [O III] + H β EWs; e.g. REBELS-15 and REBELS-39) have not necessarily assembled all of their stellar mass within the past few Myr (see Endsley et al. 2021a). We adopt a Chabrier (2003) IMF with mass limits of 0.1–$300\,M_\odot$ and apply an SMC dust prescription (Pei 1992). The metallicity and ionization parameter are allowed to lie between $-2.2 \leq \log(Z/Z_\odot) \leq 0.24$ and $-4 \leq \log U \leq -1$, respectively, both with log-uniform priors. During the fits, we only use photometry from bands redward of the Ly α break to avoid any bias due to sightline variations in IGM transmission. Details of the near-infrared photometry used for these fits will be described in Stefanon et al. (in preparation). From our BEAGLE fits, we report the median and inner 68 per cent credible interval values marginalized over the output posterior probability distribution function as determined from MULTINEST (Feroz & Hobson 2008; Feroz, Hobson & Bridges 2009). While our reported uncertainties do not account for variations in modelling assumptions, we note below how adopting non-parametric star formation history models may change our reported values.

The [C II]-detected REBELS galaxies we have thus far followed up with Binospec are all very luminous in the rest-UV with absolute UV magnitudes of $-22.7 \leq M_{UV} \leq -21.6$ (Table 2). These values correspond to 2.5–6.9 × the characteristic UV luminosity at $z \simeq 7$ ($M_{UV}^* = -20.6$; Bowler et al. 2017). As expected from their luminous nature, our REBELS targets typically represent the most massive ($\gtrsim 10^9\,M_\odot$) $z \simeq 7$ galaxies known with a median inferred stellar mass of $\log(M_*/M_\odot) = 8.9$. We note that adopting non-parametric star formation history models that disfavour strong, rapid

changes in SFR results in ∼0.5–1 dex higher inferred stellar masses for our REBELS galaxies (see Topping et al. 2022), though this does not impact any of the main conclusions in this paper. The rest-frame [O III] + H β equivalent widths (EWs) of our REBELS targets (inferred from the broad-band SEDs with our fiducial BEAGLE fits) range between 310 and 4570 Å with a median value of 940 Å (see Table 2). This is similar to the typical [O III] + H β EW inferred for the general UV-bright ($-22.5 \lesssim M_{\rm UV} \lesssim -21$) $z \sim 7$ galaxy population population (760 ± 110 Å) in Endsley et al. (2021b) where the same SED fitting procedure was adopted as above (see also Labbé et al. 2013; Smit et al. 2014; De Barros et al. 2019; Stefanon et al. 2022). Because the [O III] + H β EWs are much more directly constrained by the measured IRAC [3.6]−[4.5] colour, these inferred EWs do not change significantly if we instead utilize the results of the non-parametric star formation history fits described in Topping et al. (2022).

The inferred [O III] + H β emission strengths of our galaxies provide an estimate of their production rate of hydrogen ionizing photons, $\dot{N}_{\rm ion}$ (e.g. Chevallard et al. 2018; Tang et al. 2019; Emami et al. 2020), and in turn, their intrinsic Ly α luminosity. With these intrinsic Ly α luminosities, we determine the total escape fraction of Ly α photons from each galaxy by comparing to the measured Ly α fluxes. The intrinsic Ly α luminosity of each galaxy is calculated as $L_{\rm Ly\alpha} = 0.677 \times h \, \nu_{\rm Ly\alpha} \times \dot{N}_{\rm ion}$, where h is Planck's constant and $\nu_{\rm Ly\alpha}$ is the rest-frame frequency of Ly α. The factor of 0.677 is the fraction of hydrogen recombinations that result in the production of a Ly α photon assuming case B recombination and a temperature of 10^4 K (Osterbrock & Ferland 2006; Dijkstra 2014). We note that the $\dot{N}_{\rm ion}$ values (which are inferred from the BEAGLE fits described above) do implicitly account for dust extinction, but may be underestimated if the dust optical depth is inhomogeneous across our galaxies. In this scenario, [O III] + H β emission may be much more heavily obscured from certain star-forming regions, leading to an overestimate of the Ly α escape fractions of our galaxies. With our current low-resolution (beam ≈ 1.4 arcsec) ALMA data, we cannot yet test for such strong spatial variations in dust attenuation within our sample, though we note that a variety of dust morphologies have been seen in UV-bright $z \sim 7$–8 galaxies with higher resolution maps (Bowler et al. 2022; Schouws et al. 2022). We report the inferred Ly α escape fractions of each galaxy in Section 3 and estimate the role of the IGM in Section 5.

The total star formation rates of each galaxy are determined by summing their unobscured and obscured components. The fiducial unobscured SFRs are calculated from the UV luminosity (at 1600 Å rest-frame) adopting the conversion $\mathrm{SFR}_{\rm UV}/(M_\odot/\mathrm{yr}) = 7.1 \times 10^{-29}$ $L_{\rm UV}/(\mathrm{erg \, s^{-1} \, Hz^{-1}}$; Stefanon et al., in preparation) which results in 0.3 dex lower SFR relative to the Kennicutt (1998) conversion. This conversion ratio assumes that the galaxy of interest has been steadily forming stars for the past $\gtrsim 100$ Myr, such that the UV luminosity contribution from B stars has reached equilibrium. Accordingly, our fiducial $\mathrm{SFR}_{\rm UV}/L_{\rm UV}$ ratio may significantly underestimate the unobscured SFRs of our galaxies with very strong [O III] + H β emission (EW $\gtrsim 2000$ Å) which suggest a recent strong upturn in SFR. In Topping et al. (2022), we explicitly considered the age dependence on the $\mathrm{SFR}_{\rm UV}/L_{\rm UV}$ ratio, finding that this ratio could be approximately equal to five times larger than our fiducial value for objects with the highest [O III] + H β EWs. However, we find that this effect does not significantly impact our main conclusions (see Section 4.3).

To calculate the obscured SFRs, we adopt $\mathrm{SFR}_{\rm IR}/(M_\odot \, \mathrm{yr}^{-1}) = 1.2 \times 10^{-10} \, L_{\rm IR}/L_\odot$ (Inami et al. 2022) which yields SFRs lower by 0.16 dex relative to Kennicutt (1998). Here, the total infrared luminosities, $L_{\rm IR}$, are computed as $14\nu L_\nu$, where ν is frequency of the [C II] line and L_ν is the dust continuum flux density

determined from our ALMA observations (Sommovigo et al. 2022). For sources undetected in far-IR continuum (REBELS-03, REBELS-15, REBELS-23, and REBELS-26), we estimate their IR luminosities by calculating an average infrared excess (IRX; $L_{\rm IR}/L_{\rm UV}$) in two UV slope bins (Topping et al. 2022). That is, we split all dust-undetected REBELS objects by their median UV slope ($\beta = -2.04$) and stack the continuum data in each bin. A dust continuum detection is identified in the stack of redder galaxies and we apply the average IRX to each object in this bin (REBELS-23 and REBELS-26). The stack of bluer objects still yields a non-detection and we thus adopt upper limits on their IR luminosities from the limit on their average IRX (for REBELS-03 and REBELS-15). The resulting UV + IR SFRs of our sample span approximately 15–80 $M_\odot$ yr^{-1} (see Table 3).

3 LYMAN-ALPHA SPECTRA

We have thus far targeted Ly α from eight [C II]-detected REBELS galaxies with MMT/Binospec. In this section, we begin by detailing the Binospec spectra of the four sources in which we have confidently detected ($>7\sigma$) Ly α (Section 3.1) and then describe the EW limits of the remaining four sources that went undetected (Section 3.2). For each galaxy, we calculate the Ly α escape fraction by comparing the observed line flux to the intrinsic Ly α luminosity predicted from the BEAGLE SED fits as described in the previous section. We discuss these inferred Ly α escape fractions in Section 3.3.

3.1 Lyman-alpha detections

3.1.1 REBELS-14

REBELS-14 is an extremely UV-luminous ($M_{\rm UV} = -22.7$) galaxy in the XMM3 field at $z_{\rm [C II]} = 7.084$ (Bouwens et al. 2022; Schouws et al., in preparation), also referred to as XMM3-227436 in E21b. This source is inferred to have a stellar mass of $\log(M_*/M_\odot) = 8.7$ and its red IRAC colour ([3.6]−[4.5] $= 0.85^{+0.44}_{-0.37}$) suggests an [O III] + H β EW of 1520 Å. This is approximately twice the typical [O III] + H β EW inferred among UV-bright ($-22.5 \lesssim M_{\rm UV} \lesssim -21.25$) $z \sim 7$ galaxies in Endsley et al. (2021a, 760 ± 110 Å) where this value was determined using the same SED fitting procedures as adopted in this work.

The Binospec Ly α spectrum for REBELS-14 reveals a 19.0σ detection with a peak wavelength of 9833.3 Å (Fig. 1), corresponding to $z_{\rm Ly\alpha} = 7.089$ adopting a rest-frame wavelength of $\lambda_{\rm Ly\alpha} = 1215.67$ Å. We measure a total Ly α flux of $(21.5 \pm 1.4) \times 10^{-18}$ erg s^{-1} cm^{-2}, corresponding to an EW of 14.6 ± 3.0 Å. This EW is similar to the median value found among UV-bright ($-22.5 \lesssim M_{\rm UV} \lesssim -20.5$) galaxies at $z \simeq 7$ (10 Å; E21b), indicating that the Ly α emission strength of REBELS-14 is fairly typical. Here, we are adopting the VIRCam J-band flux density (0.59 ± 0.14 μJy) for the continuum of REBELS-14 given its [C II] redshift (see Section 2.1), and we note that the effective wavelength of the J band corresponds to a rest-frame wavelength of $\lambda_{\rm eff, rest} = 1544$ Å. The measured Ly α flux from REBELS-14 suggests a Ly α escape fraction of $f_{\rm esc, Ly\alpha} = 5.0^{+2.9}_{-1.4}$ per cent, where we use the intrinsic line luminosity predicted from the BEAGLE SED fits as described in Section 2.1. We note that the escape fraction estimates in this section include the transmission of Ly α through the galaxy (ISM and CGM) as well as the IGM. As shown in Fig. 1, a moderate-strength skyline overlaps with the redder portion of the Ly α profile from REBELS-14, possibly obscuring some of the line flux. To estimate the potential extent of the obscuration, we assume that the line flux density in this skyline region is 1.0×10^{-18} erg s^{-1} cm^{-2} Å^{-1}, a value consistent with the

Table 3. Summary of Ly α and [C II] properties of each REBELS source measured from our Binospec and ALMA observations, respectively. For sources undetected in Ly α, we quote the range of 5σ EW (and associated total Ly α escape fraction) upper limits assuming Ly α redshifts corresponding to $\Delta v_{Ly\alpha}$ = 0–800 km s^{-1} and FWHMs between 300 and 700 km s^{-1} (see Section 2.1). For REBELS-23, we report lower limits on the Ly α EW, escape fraction, and FWHM given the possibility of significant skyline obscuration on the red side of the line. For sources undetected in the ALMA continuum data, we report 3σ upper limits on their far-infrared luminosities.

ID	$z_{[C II]}$	$z_{Ly\alpha}$	Ly α EW (Å)	$f_{esc, Ly\alpha}$ (per cent)	$\Delta v_{Ly\alpha}$ (km s^{-1})	Ly α FWHM (km s^{-1})	L_{IR} ($10^{11} L_\odot$)	$L_{[C II]}$ ($10^8 L_\odot$)	SFR$_{UV+IR}$ ($M_\odot$ yr^{-1})
REBELS-03	6.969	–	<14.7–35.5	<5.2–12.6	–	–	<2.8	3.2 ± 0.6	16^{+7}_{-3}
REBELS-05	6.496	–	<3.8–4.5	<0.9–1.1	–	–	$3.3^{+2.5}_{-1.2}$	6.9 ± 0.4	53^{+23}_{-23}
REBELS-14	7.084	7.089	14.6 ± 3.0	$5.0^{+2.9}_{-1.4}$	177^{+30}_{-30}	640^{+60}_{-190}	$3.4^{+2.6}_{-1.4}$	3.7 ± 0.5	76^{+29}_{-26}
REBELS-15	6.875	6.883	3.7 ± 0.8	$0.4^{+0.2}_{-0.1}$	324^{+138}_{-34}	340^{+80}_{-140}	<3.6	1.9 ± 0.3	34^{+16}_{-9}
REBELS-23	6.645	6.650	≥13.5	≥3.3	227^{+130}_{-92}	≥330	<3.9	1.3 ± 0.2	24^{+12}_{-9}
REBELS-26	6.598	–	<5.4–6.1	<1.9–2.2	–	–	<4.8	2.0 ± 0.4	28^{+5}_{-5}
REBELS-27	7.090	–	<5.6–13.9	<3.2–8.0	–	–	$2.9^{+2.2}_{-1.1}$	6.1 ± 0.6	52^{+20}_{-20}
REBELS-39	6.845	6.849	10.0 ± 1.7	$1.7^{+0.4}_{-0.3}$	165^{+36}_{-35}	640^{+60}_{-40}	$4.3^{+3.2}_{-1.6}$	7.9 ± 1.4	88^{+30}_{-30}

flux density measured just outside both ends of the skyline. This suggests that a small fraction (14 per cent) of the total Ly α flux is obscured by this skyline which we have accounted for in the values reported above.

REBELS-14 clearly exhibits a broad asymmetric Ly α profile (Fig. 1). Given the asymmetry, we calculate the width of the line directly from the 1D spectrum, i.e. the separation between data points at half maximum flux. To account for uncertainties, we add 100 000 realizations of noise to the 1D spectrum and take the median and 68 per cent confidence intervals on the derived FWHM values across all realizations. We derive a FWHM $= 640^{+60}_{-190}$ km s^{-1}, where this value is corrected for the instrument resolution (≈68 km s^{-1}). We come back to discuss the possible physical origin of such a broad Ly α profile in Section 4.2 and the implications for Ly α transmission during reionization in Section 5.

3.1.2 REBELS-15

REBELS-15 is an extremely UV-luminous ($M_{UV} = -22.6$) galaxy in the XMM3 field at $z_{[C II]} = 6.875$ (Schouws et al., in preparation) with an inferred stellar mass of log ($M_*/M_\odot$) = 9.1. This source was identified as XMM3-504799 in E21b and exhibits a very blue IRAC colour ([3.6]–[4.5] $= -1.16^{+0.32}_{-0.43}$) suggesting an [O III] + H β EW = 4570 Å. At this redshift, [O III] λ5007 only contributes slightly to the 3.6- μm excess, requiring extremely strong H β and [O III] λ4959 emission to produce the observed IRAC colour.

Our Binospec data reveal a 7.5σ Ly α detection with a peak wavelength at 9583.2 Å corresponding to $z_{Ly\alpha} = 6.883$ (Fig. 1). The total Ly α flux is measured to be $(5.5 \pm 1.0) \times 10^{-18}$ erg s^{-1} cm^{-2} indicating an EW of 3.7 ± 0.8 Å using the VIRCam Y-band photometry ($\lambda_{eff, rest} = 1295$ Å) for the continuum flux density (0.58 ± 0.09 μJy). REBELS-15 is, thus, a relatively weak Ly α emitter among the UV-bright $z \simeq 7$ population, and is particularly weak with respect to the sub-population with strong [O III] + H β emission (EW > 800 Å; E21b). Consistent with this result, we estimate a very low total Ly α escape fraction of $0.4^{+0.2}_{-0.1}$ per cent from REBELS-15. The Ly α line profile of this source has a FWHM of 340^{+80}_{-140} km s^{-1}.

3.1.3 REBELS-23

REBELS-23 is a UV-bright ($M_{UV} = -21.6$) galaxy situated in the wide-area COSMOS field at $z_{[C II]} = 6.645$ (Schouws et al., in prepa-

ration) and was identified as COS-469100 in Endsley et al. (2021a,b). This galaxy is inferred to have a stellar mass of log ($M_*/M_\odot$) = 8.8 and its moderately blue IRAC colour ([3.6]−[4.5] $= -0.53^{+0.18}_{-0.19}$) suggests an [O III] + H β EW = 830 Å, similar to the typical value of $z \sim 7$ galaxies.

The Binospec data reveal a 7.5σ Ly α detection with a peak wavelength at 9299.3 Å corresponding to $z_{Ly\alpha} = 6.650$ (Fig. 1). From the portion of the spectrum that is unobscured by strong skylines, we measure a Ly α flux of $(9.7 \pm 1.4) \times 10^{-18}$ erg s^{-1} cm^{-2} indicating an EW of 13.5 ± 3.8 Å using the VIRCam Y-band photometry ($\lambda_{eff, rest} = 1334$ Å) for the continuum flux density (0.27 ± 0.07 μJy). The measured line flux implies $f_{esc,Ly\alpha} = 3.3^{+2.0}_{-1.3}$ per cent for REBELS-23. Due to the patch of strong skylines redward of 9305 Å, we are unable to estimate the amount of obscured line flux and thus treat the above Ly α flux, EW, and escape fraction measurements as lower limits. The Ly α profile in the unobscured portion of the spectrum has a FWHM $= 330^{+60}_{-100}$ km s^{-1}, though this width may also be underestimated due to the skylines.

3.1.4 REBELS-39

REBELS-39 is an extremely UV-luminous ($M_{UV} = -22.7$) galaxy in the COSMOS field at $z_{[C II]} = 6.845$ (Bouwens et al. 2022; Schouws et al., in preparation) and was identified as COS-862541 in Endsley et al. (2021a,b). This source has an inferred stellar mass of log ($M_*/M_\odot$) = 8.7 and a very blue IRAC colour ([3.6]−[4.5] $= -1.32^{+0.27}_{-0.34}$). The IRAC colour suggests an extremely large [O III] + H β EW of 3250 Å given that this galaxy lies at a redshift where [O III] λ5007 is only slightly transmitting through the [3.6] filter.

The Binospec data of REBELS-39 reveal a confident (15.3σ) Ly α detection with a peak wavelength of 9542.3 Å corresponding to $z_{Ly\alpha} = 6.849$ (Fig. 1). We measure a total Ly α flux of $(15.6 \pm 1.3) \times 10^{-18}$ erg s^{-1} cm^{-2}, indicating an EW of 10.0 ± 1.7 Å using the VIRCam Y-band photometry ($\lambda_{eff, rest} = 1300$ Å) for the continuum flux density (0.61 ± 0.12 μJy). While this Ly α EW is typical of UV-bright $z \simeq 7$ galaxies (E21b), the line flux from REBELS-39 implies a low total Ly α escape fraction of $1.7^{+0.4}_{-0.3}$ per cent given the extremely high [O III] + H β EW inferred for this system (3250^{+1010}_{-930} Å). The Ly α profile for REBELS-39 does overlap with a moderate-strength skyline at ≈9553 Å, though the Binospec data suggest that any obscuration is likely small. Because the observed Ly α profile is
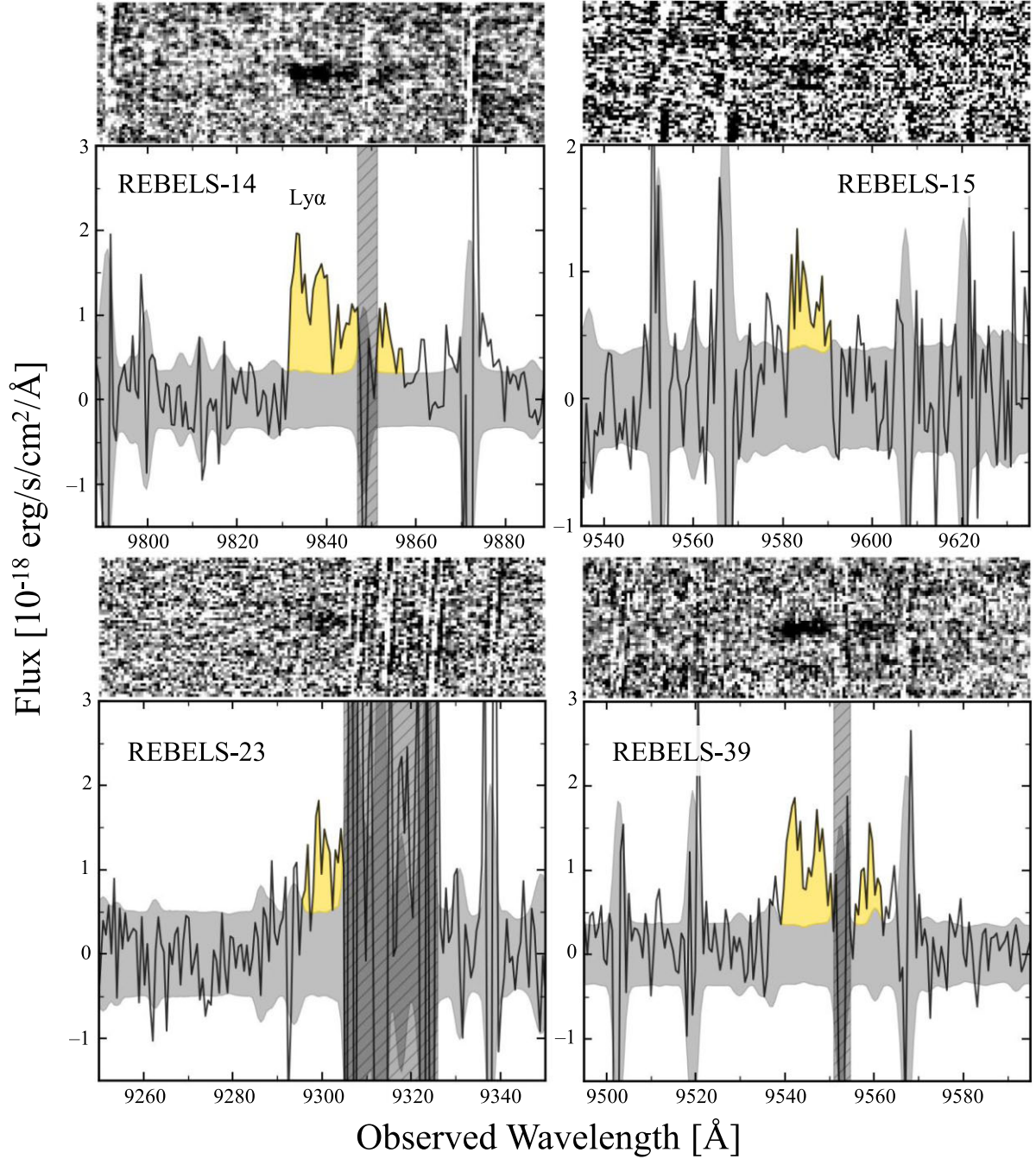
Figure 1. MMT/Binospec spectra of the four REBELS galaxies with Ly α detections. The top panels of each sub-figure show the 2D S/N maps where black is positive. The bottom panels show the 1D extraction with the 1σ noise level in grey. For clarity, we use hashed grey regions to mask portions of the 1D Ly α profiles overlapping with skylines.

consistent with zero flux density at both ends of the skyline (Fig. 1), we do not introduce a correction factor for possible flux obscuration. Similar to REBELS-14, the Ly α profile of REBELS-39 is extremely broad with FWHM = 640^{+60}_{-40} km s^{-1}.

3.2 Lyman-alpha non-detections

3.2.1 REBELS-03

REBELS-03 is a UV-bright ($M_{UV} = -21.8$) galaxy situated in the XMM1 field at $z_{[C\,II]} = 6.969$ (Bouwens et al. 2022; Schouws et al., in

preparation). This galaxy has an inferred stellar mass of log ($M_*/M_\odot$) = 8.9 and a relatively weak [O III] + H β EW of 510 Å given its flat IRAC colour ([3.6]−[4.5] = $0.01^{+0.22}_{-0.23}$). We have observed REBELS-03 for 3.75 h with MMT/Binospec with clear conditions and relatively good seeing (0.73 arcsec).

We find no indication of significant (>5σ) Ly α emission from this source after searching our Binospec spectrum in conservative wavelength range corresponding to velocity offsets betweeen −500 and 1000 km s^{-1} (Fig. 2). Due to the presence of a strong skylines around the expected wavelength of Ly α, the 5σ EW upper limit for REBELS-03 is quite poor ranging from 14.7–35.5 Å for the various
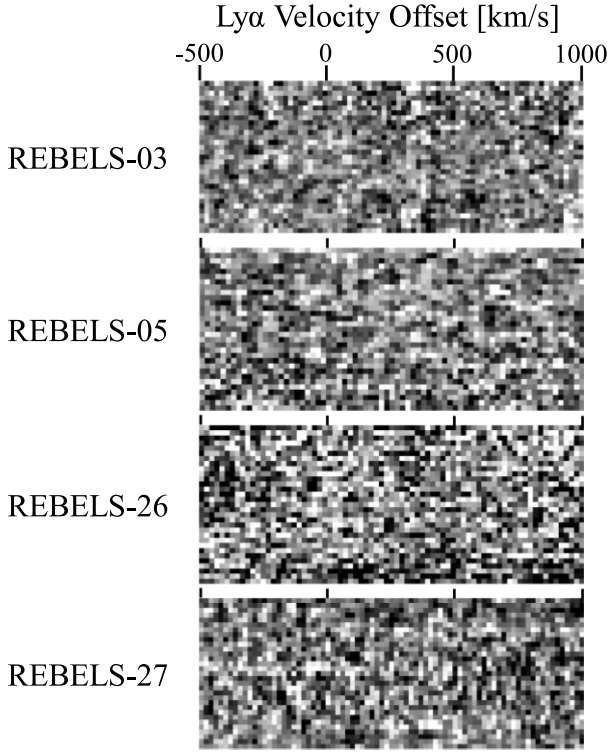
Lyα Velocity Offset [km/s]

Figure 2. Each panel shows the 2D S/N map of the MMT/Binospec spectra of each REBELS source lacking a Ly α detection ($<5\sigma$). We show wavelengths corresponding to a conservative Ly α velocity offset range of $\Delta v_{\mathrm{Ly}\alpha} = -500$ to $1000\,\mathrm{km\,s^{-1}}$ (relative to [C II]) with each panel centered on the expected spatial position of the source.

assumed velocity offsets and FWHMs (see Section 2.1). Here, we have used the UKIRT J-band photometry ($\lambda_{\mathrm{eff,\,rest}} = 1564\,\text{Å}$) for the continuum flux density (0.29 μJy). The corresponding range of 5σ limiting Ly α fluxes translate to an upper limit on the total Ly α escape fraction of $<5.2-12.6$ per cent.

3.2.2 REBELS-05

REBELS-05 is another UV-bright ($M_{\mathrm{UV}} = -21.6$) galaxy in the XMM1 field that lies at $z_{\mathrm{[C II]}} = 6.496$ (Bouwens et al. 2022; Schouws et al., in preparation) and was first identified as ID $= 118\,717$ in Bowler et al. (2014). Because this source lies at $z < 6.6$ where both IRAC bands are contaminated by strong nebular emission lines (i.e. [O III] + H β in [3.6] and H α in [4.5]), there is significant degeneracy between the inferred stellar mass and [O III] + H β EW (e.g. Schaerer & de Barros 2010). The median posterior values from BEAGLE suggest a stellar mass of $\log(M_*/M_\odot) = 8.9$ and an [O III] + H β EW of 1060 Å given its moderately blue IRAC colour ([3.6]−[4.5] $= -0.47^{+0.29}_{-0.35}$). REBELS-05 was observed using the same Binospec mask as REBELS-03 with a total exposure time of 3.75 h under clear conditions and relatively good seeing (0.73 arcsec).

We again search for Ly α at wavelengths corresponding to $\Delta v_{\mathrm{Ly}\alpha} = -500$ to $1000\,\mathrm{km\,s^{-1}}$ and find no evidence of significant emission (Fig. 2). To calculate the EW upper limit, we adopt the same set of assumed velocity offsets and FWHM values as REBELS-03 and use the VIRCam Y-band photometry ($\lambda_{\mathrm{eff,\,rest}} = 1360\,\text{Å}$) for the continuum flux density (0.35 μJy). This results in 5σ limiting EWs ranging between <3.8 and 4.5 Å. Such stringent EW constraints are

enabled by the fact that no strong skylines exist in the wavelength regime where Ly α is expected for REBELS-05. The upper limits on Ly α flux translate to $f_{\mathrm{esc,\,Ly}\alpha} < 0.9-1.1$ per cent for REBELS-05.

3.2.3 REBELS-26

REBELS-26 is a UV-bright ($M_{\mathrm{UV}} = -21.8$) galaxy in the wide-area COSMOS field at $z_{\mathrm{[C II]}} = 6.598$ (Schouws et al., in preparation) and was first identified as ID $= 104\,600$ in Bowler et al. (2014). Due to this redshift, the inferred stellar mass and [O III] + H β EW of REBELS-26 are quite degenerate similar to REBELS-05. The median posterior values from BEAGLE suggest $\log(M_*/M_\odot) = 9.1$ and [O III] + H β EW = 800 Å for REBELS-26 given its moderate IRAC colour ([3.6]−[4.5] $= -0.42^{+0.16}_{-0.17}$). We have observed this galaxy for 9.0 h with Binospec under largely clear conditions and moderate seeing on average (1.09 arcsec).

We find no indication of significant emission in our Binospec spectra for REBELS-26 at wavelengths corresponding to $\Delta v_{\mathrm{Ly}\alpha} = -500$ to $1000\,\mathrm{km\,s^{-1}}$ (Fig. 2). Because no strong skylines exist around the expected wavelength of Ly α, we derive stringent 5σ EW upper limits between 5.4–6.1 Å. Here, we have used the VIRCam Y-band photometry ($\lambda_{\mathrm{eff,\,rest}} = 1342\,\text{Å}$) for the continuum flux density (0.37 μJy). The total Ly α escape fraction of this system is inferred to be $<1.9-2.2$ per cent using the range of 5σ upper limits on the line flux.

3.2.4 REBELS-27

REBELS-27 is another UV-luminous ($M_{\mathrm{UV}} = -21.9$) galaxy identified across the wide-area COSMOS field located at $z_{\mathrm{[C II]}} = 7.090$ (Bouwens et al. 2022; Schouws et al., in preparation). This source was referred to as UVISTA-Y-004 in Stefanon et al. (2017, 2019) and UVISTA-301 in Bowler et al. (2020). It has an inferred stellar mass of $\log(M_*/M_\odot) = 9.5$ and its flat IRAC colour ([3.6]−[4.5] $= 0.10^{+0.20}_{-0.22}$) suggests relatively weak [O III] + H β emission (EW = 310 Å). We have observed REBELS-26 for 4.5 h with Binospec under clear conditions and moderate seeing (0.94 arcsec).

After searching for Ly α at wavelengths corresponding to $\Delta v_{\mathrm{Ly}\alpha} = -500$ to $1000\,\mathrm{km\,s^{-1}}$, we find no indication of significant line emission (Fig. 2). The 5σ upper limiting EW ranges between 5.6–13.9 Å given that a moderate-strength skyline impacts part of the relevant wavelength regime. For the continuum flux density, we use the VIRCam J-band photometry ($\lambda_{\mathrm{eff,\,rest}} = 1543\,\text{Å}$) measurement of 0.47 μJy. The total Ly α escape fraction from REBELS-27 is inferred to be $<3.2-8.0$ per cent.

3.3 Lyman-alpha escape fractions from REBELS galaxies

It is well-established that luminous, UV-selected galaxies at $z \sim 2-3$ tend to have low Ly α escape fractions (≈ 5 per cent) due to their substantial dust content and high H I covering fractions (e.g. Hayes et al. 2010; Steidel et al. 2011; Ciardullo et al. 2014; Matthee et al. 2016; Weiss et al. 2021). It is, however, much less clear how efficiently Ly α photons are able to escape from galaxies at $z > 6$. On average, these very early systems are found to be much bluer with considerably larger sSFRs relative to typical galaxies at $z \sim 2$ (e.g. Stark et al. 2013; Bouwens et al. 2014; Béthermin et al. 2015; Salmon et al. 2015; Strait et al. 2020; Stefanon et al. 2022), suggesting they may have physical conditions more conducive to efficient Ly α escape. Our REBELS sample enables us to investigate this possibility among the most UV-luminous ($-22.7 \leq M_{\mathrm{UV}} \leq -21.6$)

and massive ($M_* \gtrsim 10^9\,M_\odot$) galaxies at $z \sim 7$. In the previous sub-section, we quantified the Lyα escape fraction of each of our Binospec-targeted REBELS galaxies and the resulting values are summarized in Table 3. Notably, the [C II] systemic redshifts enable us to place confident upper limits on the escape fraction for sources which went undetected in Lyα since we know whether their Lyα profiles may overlap with strong skylines.

None of the eight UV-luminous ($-22.7 \leq M_{\rm UV} \leq -21.6$) $z \sim 7$ REBELS galaxies which we have targeted with Binospec appear to show strong Lyα emission (EW > 25 Å). This is particularly striking given that a large fraction (75 per cent) of these systems are inferred to exhibit high EW [O III] + Hβ emission (≥ 800 Å) implying efficient production of hydrogen ionizing photons (Chevallard et al. 2018; Tang et al. 2019; E21b). As expected from this result, we find that at least half our REBELS galaxies have low Lyα escape fractions of <2.5 per cent (Table 3). Even after correcting these values for Lyα transmission through the IGM ($T \approx 50-80$ per cent; see Section 5), we find that only 3–4 per cent of Lyα photons typically escape our REBELS galaxies, comparable to that of similarly massive ($\gtrsim 10^9\,M_\odot$) systems at $z \sim 2-3$. This suggests that much of the Lyα photons are resonantly trapped within the galaxy, likely due in part to a large column density of neutral hydrogen close to the systemic velocity (e.g. Neufeld 1990; Mas-Hesse et al. 2003; Verhamme, Schaerer & Maselli 2006; Steidel et al. 2010) though destruction by dust likely plays a significant role as well.

While our Binospec-targeted REBELS galaxies are blue in the rest-UV (median $\beta = -1.94$), our ALMA data none the less indicate the presence of substantial dust reservoirs in many of these systems ($M_{\rm dust} \sim 10^7\,M_\odot$; Dayal et al. 2022; Ferrara et al. 2022) which likely contribute significantly to the absorption of their Lyα photons (see e.g. Behrens et al. 2019). It may be expected that we find a correlation between Lyα escape fraction and far-infrared luminosity among our REBELS sample. In reality, such a trend is challenging to recover with our current data set for two reasons. First, our ALMA data only provide shallow upper limits on the far-infrared luminosity for sources undetected in dust continuum (see Table 3), allowing for the possibility of large dust masses within these systems. Secondly, our sample is limited by small statistics and a narrow dynamic range in Lyα escape fraction ($\lesssim 5$ per cent). Indeed, we find that when we separate our sample by low (<2.5 per cent) and moderate (2.5–5 per cent) Lyα escape fractions, we do not find a clear difference in the average far-infrared luminosity. The two sources with moderate Lyα escape fractions (REBELS-14 and REBELS-23) have far-infrared luminosities of 3.4×10^{11} and $<3.9 \times 10^{11}\,L_\odot$, respectively, where we quote 3σ upper limits for non-detected objects. Our ALMA data are consistent with similar far-infrared luminosities among the four galaxies with low (<2.5 per cent) Lyα escape fractions within current sensitivity limits ($\leq 3.3 \times 10^{11}$ to $4.3 \times 10^{11}\,L_\odot$; see Table 3). Here, we are ignoring the two sources with Lyα escape fraction upper limits above 2.5 per cent (i.e. REBELS-03 and REBELS-27) since we cannot determine which bin these galaxies fall into. Further Lyα observations of the REBELS sample as well as improved constraints on their far-infrared luminosity would enable a better assessment of the impact of dust on Lyα escape among massive ($\gtrsim 10^9\,M_\odot$) reionization-era galaxies.

4 ANALYSIS

All of the galaxies considered in this work have ALMA detections of their [C II] 158-μm emission (Bouwens et al. 2022). In this section, we first use the [C II] data to measure the Lyα velocity offsets of

the four galaxies with Binospec detections, and discuss our results in context of the literature (Section 4.1). We then consider how the broad Lyα line widths of these four $z \simeq 7$ REBELS galaxies likely assist in enhancing transmission through the IGM (Section 4.2). Finally, we explore whether our sample shows any evidence of a connection between Lyα EW and [C II] luminosity at fixed SFR (Section 4.3).

4.1 Lyman-alpha velocity offsets of UV-bright z > 6 galaxies

An increasing number of observations have demonstrated that UV-bright ($M_{\rm UV} \lesssim -21$) galaxies do not show strong evolution in their Lyα line strengths between $z \sim 6$ and $z \sim 7$ (Ono et al. 2012; Stark et al. 2017, E21b) even as the IGM neutral fraction rises rapidly over this time period (e.g. McGreer et al. 2015; Davies et al. 2018; Wang et al. 2020; Yang et al. 2020). This indicates that Lyα photons from UV-luminous $z \sim 7$ galaxies are somehow able to avoid strong resonant interactions with the surrounding intergalactic H I. One possible explanation is that their photons often escape the CGM at velocities significantly redward of systemic ($>100\,{\rm km\,s^{-1}}$), placing them beyond the resonant core and well into the damping wing where transmission is greatly enhanced. While such large Lyα velocity offsets are commonly observed among similarly bright galaxies at $z \sim 2-3$ (Hashimoto et al. 2013; Erb et al. 2014; Shibuya et al. 2014), a statistical analysis at $z > 6$ has been hindered by observational challenges. To date, only a small fraction of UV-luminous $z > 6$ galaxies have been detected in Lyα, and much fewer have detections of a second emission line tracing the systemic redshift (e.g. [C II]158 μm). Here, we help address this issue using new [C II] detections of UV-luminous $z \geq 6.5$ galaxies from the ALMA REBELS program (Bouwens et al. 2022).

We have thus far detected Lyα emission in four REBELS galaxies at $z_{\rm [C II]} = 6.6 - 7.1$ (REBELS-14, REBELS-15, REBELS-23, and REBELS-39; Section 3.1). All four of these systems are in the UV luminosity range where Lyα transmission appears to not be strongly evolving between $z \sim 6$ and $z \sim 7$ ($M_{\rm UV} \sim -22$). We compute the Lyα velocity offsets of these galaxies using systemic redshifts corresponding to the central [C II] wavelength from Gaussian fits to the 1D ALMA spectra (Schouws et al., in preparation). The Lyα redshifts are measured from the wavelength of peak line flux (see Section 3.1) similar to the approach of many previous studies (Maiolino et al. 2015; Stark et al. 2015, 2017; Carniani et al. 2017, 2018b; Mainali et al. 2017; Matthee et al. 2020). From our redshift measurements, we calculate Lyα velocity offsets of 177, 324, 227, and 165 km s^{-1} for REBELS-14, REBELS-15, REBELS-23, and REBELS-39, respectively (see Table 3). Our results indicate that a significant portion of Lyα photons from these four UV-luminous ($M_{\rm UV} \sim -22$) $z \sim 7$ galaxies are emerging well into the damping wing (average velocity offset of 223 km s^{-1}) where IGM transmission is significantly boosted.

To place our results in the context of previous studies, we consider the sample of $z > 6$ velocity offset measurements from the literature. Here, we only include measurements derived from secure (S/N > 5) Lyα detections where the bluer side of the observed Lyα emission feature (containing the peak of the profile) is not significantly impacted by skylines. We also ignore measurements derived from systemic line detections that were considered tentative in their published works. With our REBELS sample, we have nearly doubled the number of Lyα velocity offset measurements among extremely UV-luminous ($M_{\rm UV} < -22$) Lyman-break selected galaxies at $z > 6$, boosting available statistics from $N = 4$ to 7 (see Table 4; Willott et al. 2015; Stark et al. 2017; Hashimoto et al. 2019). These seven extremely bright galaxies have an average velocity offset of

Table 4. Summary of literature measurements of Ly α velocity offsets at $z > 6$ including those from this work. We only consider measurements derived from galaxies where the Ly α feature is detected at S/N > 5 and where the bluer side of the observed Ly α emission feature is not significantly impacted by skylines. We also ignore measurements derived from systemic line detections that were considered tentative in their published works.

ID	z	M_{UV}	$\Delta v_{Ly\alpha}$ (km s^{-1})	Ly α EW (Å)	References
			Lyman-break selected galaxies		
CLM1	6.17	-22.8	430	50	Cuby et al. (2003), Willott et al. (2015)
WMH5	6.07	-22.7	504	13	Willott et al. (2013, 2015)
REBELS-14	7.08	-22.7	177	15	This work
REBELS-39	6.85	-22.7	165	10	This work
REBELS-15	6.88	-22.6	324	4	This work
B14-65666	7.15	-22.4	772	4	Furusawa et al. (2016), Hashimoto et al. (2019)
EGS-zs8-1	7.72	-22.1	340	21	Oesch et al. (2015), Stark et al. (2017)
COS-zs7-1	7.15	-21.9	135–420^a	15–28^a	Pentericci et al. (2016), Laporte et al. (2017), Stark et al. (2017)
COSMOS24108	6.62	-21.7	240	27	Pentericci et al. (2016, 2018)
REBELS-23	6.64	-21.6	227	14	This work
NTTDF6345	6.70	-21.6	110	15	Pentericci et al. (2011, 2016)
UDS16291	6.64	-21.0	110	6	Pentericci et al. (2016, 2018)
BDF-3299	7.11	-20.5	71	50	Vanzella et al. (2011), Maiolino et al. (2015), Carniani et al. (2017)
RXJ2248-ID3	6.11	-20.2^b	235	40	Mainali et al. (2017)
A383-5.2	6.03	-19.3^b	85–120^c	138	Stark et al. (2015), Knudsen et al. (2016)
			Narrowband-selected Lyman-alpha Emitting Galaxies		
VR7	6.53	-22.4	213	38	Matthee et al. (2019, 2020)
CR7	6.60	-22.2	167	211	Sobral et al. (2015), Matthee et al. (2017)
Himiko	6.59	-21.9	145	78	Ouchi et al. (2013), Carniani et al. (2018b)

Notes. ^{a} Different Ly α redshifts and EWs are reported for COS-zs7-1 in Pentericci et al. (2016), Laporte et al. (2017), and Stark et al. (2017). We list the corresponding range of velocity offsets and EWs found between the three works.
^{b} The UV magnitudes of RXJ2248-ID3 and A383-5.2 have been corrected for gravitational lensing adopting $\mu = 5.5$ and 7.3, respectively (Stark et al. 2015; Mainali et al. 2017).
^{c} For A383-5.2, we report the Ly α velocity offset measured using the [C III] $\lambda 1909$ redshift from Stark et al. (2015) and the [C II]158 μm redshift from Knudsen et al. (2016). For both measurements, we adopt the Ly α redshift from Stark et al. (2015).

387 km s^{-1}. Moreover, each exhibits $\Delta v_{Ly\alpha} > 100$ km s^{-1} indicating that such large values are very common (if not ubiquitous) in the extremely UV-luminous $z > 6$ population (see Fig. 3).

We now compare the velocity offsets seen among the extremely UV-luminous ($M_{UV} < -22$) $z > 6$ galaxy population to those in the $z \sim 5$ ALMA ALPINE survey (Le Fèvre et al. 2020). Using the ALPINE DR1 catalogue (Béthermin et al. 2020; Cassata et al. 2020; Faisst et al. 2020), we find that there are twenty $M_{UV} < -22$ galaxies with both Ly α and [C II] redshift measurements at $z = 4.4-5.7$. These 20 galaxies exhibit Ly α velocity offsets spanning -192 km s$^{-1} \leq \Delta v_{Ly\alpha} \leq 520$ km s^{-1} with an average of 193 km s^{-1}. This average value is substantially lower than that seen among the luminosity-matched $z > 6$ sample (387 km s^{-1}). However, we note that the velocity offsets of these ALPINE galaxies will be weighted towards low values given their relatively high Ly α EWs. It has been shown that galaxies with larger Ly α EWs tend to exhibit smaller velocity offsets, both at $z \sim 2-3$ (e.g. Hashimoto et al. 2013; Erb et al. 2014) as well as within the $z \sim 5$ ALPINE sample (Cassata et al. 2020), likely in part because lower H I column densities near systemic leads to more efficient Ly α escape from the galaxy at $\Delta v_{Ly\alpha} \sim 0$ km s^{-1}. According to the ALPINE catalogue, 45 per cent (9/20) of the extremely UV-luminous galaxies with velocity offset measurements show strong Ly α emission (EW > 25 Å), a considerably larger fraction than that typically reported among Lyman-break selected UV-bright ($M_{UV} < -20.5$) galaxies at $z \sim 5$ (≈ 25 per cent; e.g. Stark, Ellis & Ouchi 2011; Cassata et al. 2015). This is to be expected given that the ALPINE galaxies were partially assembled from a sample of narrow-band selected Ly α emitters (Faisst et al. 2020). We note that the sample of seven
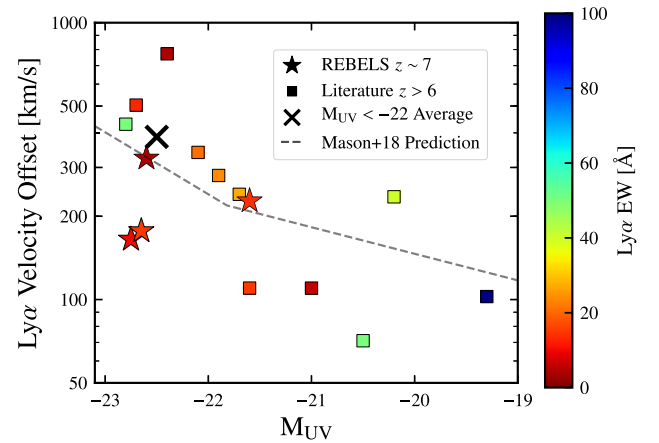

Figure 3. Ly α velocity offsets measurements versus M_{UV} among Lyman-break selected galaxies at $z > 6$. The stars show measurements from the REBELS sample while squares show additional measurements from the literature where points are colour-coded by the Ly α EW. All values shown here are tabulated in Table 4 where, in cases when a property has multiple reported values across various works, we plot the average of those reported values. The black cross shows the average velocity offset of 387 km s^{-1} measured among extremely UV-luminous ($M_{UV} < -22$) $z > 6$ galaxies while the black dashed line shows the predicted relation between the average Ly α velocity offset and UV magnitude at $z = 7$ from Mason et al. (2018a). Available $z > 6$ velocity offset measurements at the fainter end ($M_{UV} \geq -20.5$) may be biased low given the relatively high Ly α EWs (40–138 Å) of these three objects.

extremely UV-luminous $z > 6$ galaxies considered above exhibit fairly representative Ly α EWs with respect to the broader UV-bright $z \sim 6-7$ population (E21b), suggesting that their Ly α velocity offsets will also be representative. Only 14 per cent (1/7) of these systems show strong Ly α, comparable to that typically seen among UV-bright ($M_{UV} < -20.5$) Lyman-break selected $z \sim 6-7$ samples (≈ 10 per cent; Stark et al. 2011; Ono et al. 2012; Schenker et al. 2014; De Barros et al. 2017; Pentericci et al. 2018). Moreover, the median Ly α EW of these seven galaxies (13 Å) is very similar to that inferred for the larger UV-bright $z \sim 7$ population in E21b (10 ± 3 Å).

Many studies have established that faint ($-20 \lesssim M_{UV} \lesssim -18$) galaxies exhibit a strong, rapid decline in Ly α emission strength at $z > 6$ (e.g. Schenker et al. 2014; Pentericci et al. 2018; Fuller et al. 2020), in contrast to the bright ($M_{UV} \lesssim -21$) population. This luminosity dependence on Ly α transmission could arise (at least in part) from smaller velocity offsets among fainter $z > 6$ galaxies, as may be expected if lower mass systems have less H I gas near systemic velocity (e.g. Steidel et al. 2010; Erb et al. 2014). However, it is not clear that this is the case from existing data. There are currently only three intrinsically faint ($M_{UV} \geq -20.5$) galaxies at $z > 6$ with robust Ly α velocity offset measurements (see Fig. 3 and Table 4; Maiolino et al. 2015; Stark et al. 2015; Carniani et al. 2017; Mainali et al. 2017). This limited sample size is largely the result of challenges in obtaining multiline detections of faint reionization-era systems. While all three galaxies do show velocity offsets smaller than the average of UV-luminous ($M_{UV} < -22$) systems (Table 4), their Ly α emission is clearly unusual. With EWs of 40–138 Å, these galaxies fall into the rare ($\sim$5–20 per cent) sub-class of very strong Ly α emitters among the faint $z \sim 6-7$ population (Pentericci et al. 2018). Because galaxies with higher EW Ly α emission typically exhibit smaller velocity offsets (at least at $z < 6$; e.g. Hashimoto et al. 2013; Erb et al. 2014; Cassata et al. 2020), the measured offsets of these three faint galaxies may be biased towards low values. Further observations of faint $z > 6$ galaxies with more typical Ly α emission (EW $\lesssim 10$ Å; Pentericci et al. 2018) are required to better assess the average velocity offset of this population.

4.2 Lyman-alpha line widths of UV-luminous z > 6 galaxies

Along with velocity offsets, the Ly α line widths of $z > 6$ galaxies determine how efficiently their photons transmit through a partially neutral IGM. Galaxies with broader Ly α profiles emit a larger fraction of flux at high velocities where the damping wing absorption is weaker, thereby boosting IGM transmission. In this subsection, we discuss the Ly α line widths of our UV-luminous ($M_{UV} \sim -22$) REBELS galaxies and compare to those of fainter sources.

All four REBELS galaxies with Binospec detections display broad Ly α lines with FWHM > 300 km s^{-1} (see Table 3). Two of these systems (REBELS-14 and REBELS-39) show extremely wide Ly α profiles (FWHM ≈ 650 km s^{-1}) with significant emission detected ≈ 750 km s^{-1} relative to systemic (see Fig. 4). At these velocities, Ly α photons are pushed far into the damping wing where the absorption cross-section is nearly 2 orders of magnitude less than that at 100 km s^{-1} (Dijkstra 2017). The presence of Ly α flux at such large velocities undoubtedly enhances the visibility of these UV-luminous galaxies in a mostly neutral IGM.

We can obtain more stringent constraints on this population looking at all UV-selected $z > 6$ galaxies with Ly α FWHM measurements. Here, we only consider S/N > 7 Ly α detections where the measured width is not strongly impacted by OH skylines. In the sample of six UV-luminous ($M_{UV} < -22$) galaxies, we find an

average Ly α FWHM of 450 km s^{-1}, with values ranging from 310–640 km s^{-1} (see Fig. 5a and Table 5, Cuby et al. 2003; Willott et al. 2013; Oesch et al. 2015). If these large line widths are to preferentially boost Ly α transmission with respect to less luminous galaxies, we would expect to see a luminosity-dependent trend in the FWHM of Ly α. In the nine UV-selected $z > 6$ galaxies with low luminosities ($M_{UV} \geq -20.5$) and published Ly α line width measurements, we find FWHMs ranging from 130 to 285 km s^{-1} with an average of 185 km s^{-1} (Table 5; Nagao et al. 2005; Vanzella et al. 2011, 2014; Stark et al. 2015; Mainali et al. 2017; Hoag et al. 2019; Pelliccia et al. 2021). These are uniformly smaller than the widths of the more luminous systems considered in this paper, hinting at a luminosity-dependent trend (see Fig. 5a).

The presence of such broad Ly α widths in the REBELS galaxies is not necessarily surprising. UV-luminous galaxies at $z \simeq 7$ are likely to have neutral outflows with large column densities spanning a wide range of velocities, as are commonly seen in similarly luminous galaxies at lower redshifts (e.g. Shapley et al. 2003; Verhamme et al. 2008; Steidel et al. 2010). The Ly α profiles in these systems will accordingly take on broader widths from back-scattered emission off the far side of the outflowing gas. Such resonant scattering effects surely play a significant role in transferring Ly α photons to the large velocities described above.

Our ALMA data suggests another factor may also contribute to the broad line widths. The two systems in our sample exhibiting extremely broad Ly α emission (REBELS-14 and REBELS-39) also show atypically broad [C II] profiles with FWHM = 300–520 km s^{-1} (see Table 5; cf. the median FWHM = 220 km s^{-1} among all 24 [C II]-detected REBELS galaxies; Schouws et al., in preparation), indicating that the broadest Ly α emission is seen from galaxies with ISM reservoirs spanning the largest range of velocities. This is also true in the wider literature sample (see Fig. 5b). If we consider the seven UV-selected $z > 6$ galaxies with Ly α and [C II] FWHM measurements (Table 5), the three with the largest [C II] FWHM (≥ 300 km s^{-1}, WMH5, REBELS-39, REBELS-14) have an average Ly α FWHM of 530 km s^{-1} (Willott et al. 2013, 2015). The four with lower [C II] FWHM ($\lesssim 160$ km s^{-1}, CLM1, REBELS-15, BDF-3299, A383) have an average Ly α FWHM of just 270 km s^{-1} (Cuby et al. 2003; Vanzella et al. 2011; Maiolino et al. 2015; Stark et al. 2015; Willott et al. 2015; Knudsen et al. 2016).

The connection between the Ly α and [C II] line widths suggests that the velocity dispersion of the gas powering the line emission is likely playing a significant role in driving the FWHM of Ly α emission. The origin of the very broad [C II] emission is still not entirely clear (Kohandel et al. 2019, 2020). High-resolution imaging from *HST* potentially gives some insight, revealing that UV-luminous ($M_{UV} < -22$) $z \simeq 7$ galaxies tend to be composite systems comprised of several bright clumps separated by $\simeq 2-5$ kpc (Sobral et al. 2015; Bowler et al. 2017; Matthee et al. 2019). These clumps are likely to have significant peculiar motions (>100–500 km s^{-1}) given their separation and the dynamical masses of their host galaxies ($\simeq 1 \times 10^{10}$–3×10^{10} M$_\odot$), consistent with ALMA observations for a subset of these sources (Jones et al. 2017; Matthee et al. 2017; Carniani et al. 2018a; Hashimoto et al. 2019). At the spatial resolution of the REBELS [C II] maps (beam ≈ 7 kpc), these putative clumps are mostly blended, which can naturally produce the broad (and potentially multipeaked) [C II] profiles seen in our data (Kohandel et al. 2019). If each clump of gas is also powering Ly α emission, we would expect the intrinsic Ly α profile to start out fairly broad in these luminous galaxies, mirroring the [C II] line profile. Resonant scattering off of the outflowing gas will further broaden the line and shift it to higher velocities.
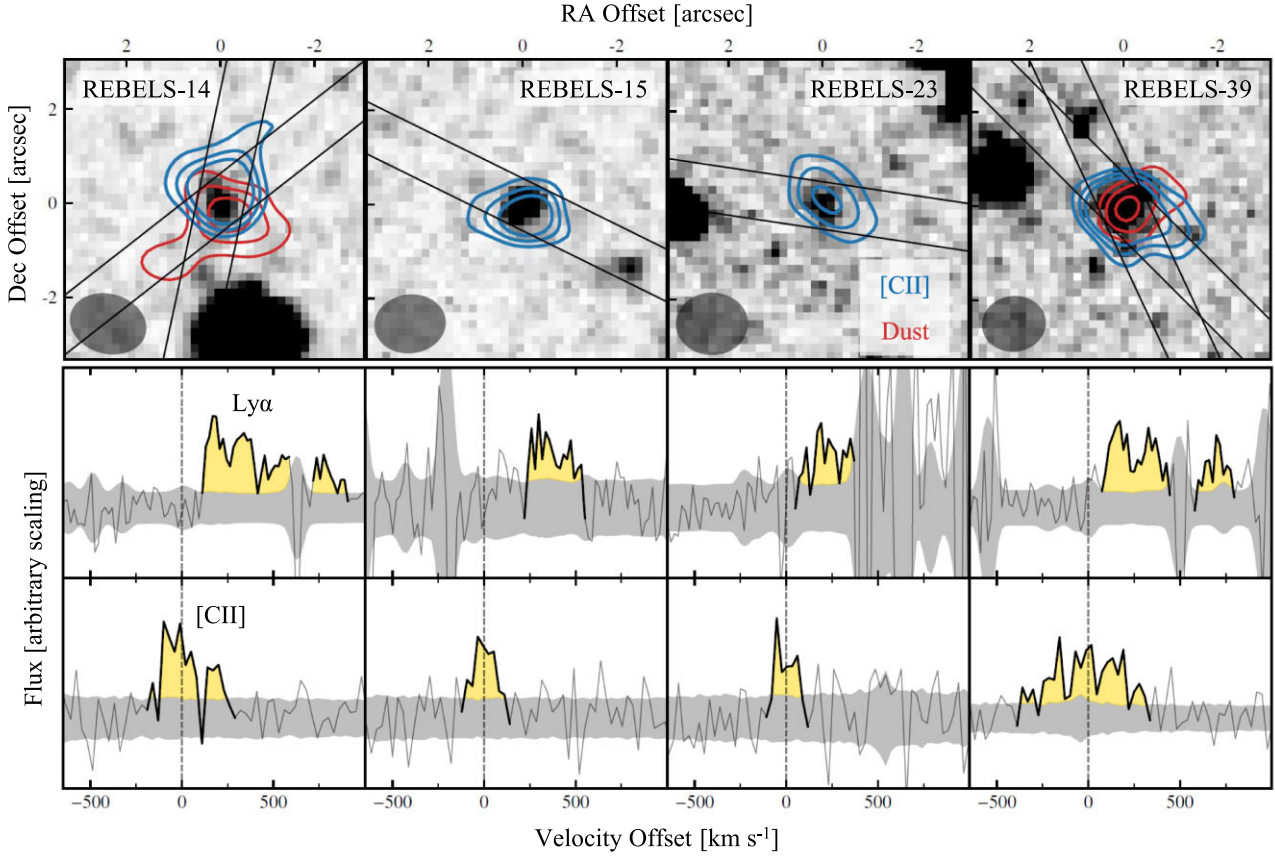
Figure 4. Top panel: ALMA [C II] (blue) and dust continuum (red) contour maps overlaid on the near-infrared χ^2 image of each REBELS source detected in Ly α. We show the 2σ, 3σ, and 4σ contours of detections within 1 arcsec of the source centroid from near-infrared imaging. The Binospec slit positions are shown with black lines where REBELS-14 and REBELS-39 were observed with two different slit orientations. Also shown is the ALMA beam size in the lower left-hand of each panel. Middle panel: Ly α velocity profiles of each source using the systemic redshift measured from [C II]. We highlight portions of the profiles free of skyline obscuration with detected flux. Bottom panel: [C II] velocity profiles of each source. Format is similar to the middle panels.
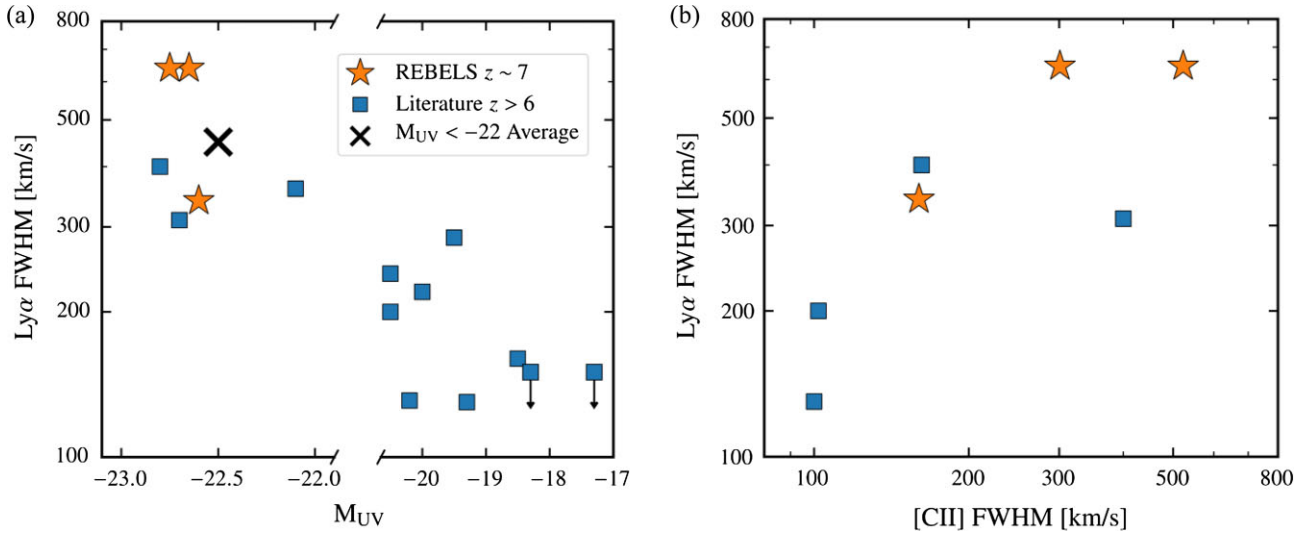
Figure 5. (a) Ly α FWHM versus M_{UV} among Lyman-break selected galaxies at $z > 6$. The stars represent measurements from the REBELS sample while squares show additional measurements from the literature. All values shown here are tabulated in Table 5 and we only consider sources with $M_{UV} < -22$ or ≥ -20.5 to explore evidence of a luminosity dependence on Ly α FWHM at $z > 6$. Current data suggest that brighter $z > 6$ sources commonly exhibit larger Ly α FWHMs, with an average FWHM of 450 km s^{-1} measured among extremely UV-luminous ($M_{UV} < -22$) galaxies (black cross). (b) Measurements of Ly α FWHM versus [C II] FWHM when available among this same sample (see Table 5). These existing data suggest that the broadest Ly α emission is seen from galaxies with ISM reservoirs spanning the largest range of velocities.

Table 5. Literature measurements of Ly α FWHM among Lyman-break selected galaxies at $z > 6$. We consider only those with either $M_{UV} \leq -22$ or ≥ -20.5 (separated by the horizontal line) to explore a luminosity-dependent trend. This sample is limited to S/N > 7 Ly α detections where the measured line width is not strongly impacted by skylines. [C II] FWHM measurements are also listed where available.

ID	z	M_{UV}	Ly α EW (Å)	Ly α FWHM (km s^{-1})	[C II] FWHM (km s^{-1})	References
CLM1	6.17	−22.8	50	400	162	Cuby et al. (2003), Willott et al. (2015)
WMH5	6.07	−22.7	13	310	400	Willott et al. (2013, 2015)
REBELS-39	6.85	−22.7	10	640	523	This work
REBELS-14	7.08	−22.7	15	640	301	This work
REBELS-15	6.88	−22.6	4	340	160	This work
EGS-zs8-1	7.72	−22.1	21	360	–	Oesch et al. (2015)
BDF-521	7.01	−20.5	64	240	–	Vanzella et al. (2011)
BDF-3299	7.11	−20.5	50	200	102	Vanzella et al. (2011), Maiolino et al. (2015)
RXJ2248-ID3	6.11	−20.2[a]	40	131	–	Mainali et al. (2017)
SDFJ132442	6.04	−20.0	236	220	–	Nagao et al. (2005)
RELICS-DP7	7.03	−19.5[a]	342	285	–	Pelliccia et al. (2021)
A383-5.2	6.03	−19.3[a]	138	130	100	Stark et al. (2015), Knudsen et al. (2016)
MACS0744-064	7.15	−18.5[a]	58	160	–	Hoag et al. (2019)
macs0717_0859	6.39	−18.3[a]	45	≲150	–	Vanzella et al. (2014)
macs0717_1730	6.39	−17.3[a]	32	≲150	–	Vanzella et al. (2014)

Note. [a] We adopt magnification factors of $\mu = 5.5, 1.15, 7.3, 3.2, 6.9,$ and 17.3 for RXJ2248-ID3, RELICS-DP7, A383-5.2, MACS0744-064, macs0717_0859, and macs0717_1730, respectively as stated by the corresponding references listed in the table.

While fainter systems are likely to also breakup into clumps, these less massive and more compact galaxies should have smaller velocity dispersions, leading to narrower initial line widths (before transfer through the outflowing gas). If the outflowing gas of these faint galaxies also has smaller velocities and lower column densities, it will further contribute to narrow Ly α widths. This physical picture will soon be easily testable with higher spatial resolution ALMA maps and *JWST* IFU observations of Ly α and non-resonant nebular lines. If shown to be true, it would suggest that the substantial peculiar motions of clumps in very luminous galaxies will impact the observed Ly α profile and in turn the atypical visibility of Ly α emission lines in this population. It would also suggest that when multiple spectral peaks in Ly α are observed, they do not always imply that one of the peaks is blueward of the systemic redshift (e.g. Matthee et al. 2018; Meyer et al. 2021). Such blue Ly α peaks are exciting as they imply a low covering fraction of neutral gas, potentially an indicator of Lyman-continuum leakage (e.g. Henry et al. 2015; Verhamme et al. 2015; Jaskot et al. 2019; Gazagnes et al. 2020; Hayes et al. 2021). We suggest that systemic redshifts (as provided by [C II]) are critical for interpreting the Ly α profiles, as multiple peaks can arise naturally from blended clumps of gas in large composite systems.

Our Binospec data may be providing evidence of multipeaked Ly α profiles arising from separate gas clumps in extremely luminous $z \simeq 7$ galaxies. As can be seen in Fig. 6, the Ly α profiles of both REBELS-14 and REBELS-39 tentatively show multiple peaks of emission even though all flux is detected redward of the systemic velocity from [C II]. In the Ly α spectra of REBELS-14, there are potentially two peaks at velocities of approximately 220 and 380 km s^{-1} relative to systemic where this separation of 160 km s^{-1} is more than twice the resolution of our Binospec data (≈ 68 km s^{-1}). There is also a possible third Ly α peak in REBELS-14 giving rise to the flux seen on both sides of the moderate-strength skyline at ≈ 680 km s^{-1} relative to systemic. The Ly α profile of REBELS-39 shows a similar structure. There are possibly two separate peaks at velocities of approximately 110 and 300 km s^{-1} relative to systemic along with a potential third peak at ≈ 670 km s^{-1}. We acknowledge that the presence of skylines and the current S/N of our data leaves significant uncertainty in the true number of Ly α peaks for each REBELS source, though we note that lower redshift ($z \sim 2-4$) galaxies have been shown to exhibit

significant spatial variations in their Ly α profiles (e.g. Erb, Steidel & Chen 2018; Claeyssens et al. 2019; Leclercq et al. 2020).

To assess the plausibility of these potential multipeak Ly α solutions, we fit the 1D spectra of REBELS-14 and REBELS-39 assuming three peaks of emission. During the fits, we assume that the bluest peak is a half-Gaussian while the redder two peaks are symmetric Gaussians (due to less attenuation by the IGM/CGM at higher velocities). Each peak component is convolved with the instrument resolution and regions overlapping with strong skylines are masked during the fits. For comparison, we also consider single-peak profile solutions treated as a half-Gaussian convolved with the instrument resolution. The triple-peak Ly α models are able to reproduce the observed line shapes for both REBELS-14 and REBELS-39, yielding best-fitting reduced χ^2 values of 0.50 and 0.66, respectively. The single-peak models provide a poorer match to the data with best-fitting reduced χ^2 values of 1.16 and 1.20, respectively, where here we are accounting for the fact that the triple-peak fits have more degrees of freedom. None the less, deeper spectra will be required to verify whether multiple emission peaks (all redward of systemic velocity) are indeed present in the Ly α profiles of these two extremely luminous ($M_{UV} = -22.7$) $z \simeq 7$ galaxies. If shown to be true, these separate Ly α peaks could support the presence of multiple gas clumps with large peculiar motions within each galaxy (cf. Park et al. 2021), as may be further evidenced by their possible multipeaked [C II] profiles (Fig. 4). Such a physical picture would clearly help explain the extremely broad Ly α emission (FWHM $\approx$ 640 km s^{-1}) observed from these two galaxies, though it is unclear in this picture why the bluest Ly α peak is the strongest given that it lies closest to systemic where the H I column density is perhaps the largest.

4.3 The dependence of [C II] production on Lyα EW at z ∼ 7

The first ALMA surveys targeting $z \gtrsim 7$ galaxies resulted in very few [C II] detections (Ouchi et al. 2013; Ota et al. 2014; Maiolino et al. 2015; Schaerer et al. 2015), even though the observation depths were calibrated to local empirical relations between [C II] luminosity and SFR (e.g. De Looze et al. 2014). It has been proposed that this

so-called [C II] deficit was in part due to the selection bias towards $z \gtrsim$ 7 galaxies with strong Ly α emission which had known spectroscopic redshifts (e.g. Pentericci et al. 2016; cf. Pallottini et al. 2019; Carniani et al. 2020). These strong Ly α emitters may be expected to show weaker [C II] at fixed SFR due to e.g. lower metallicities relative to the typical high-redshift galaxy population (e.g. Ouchi et al. 2013; Maiolino et al. 2015; Vallini et al. 2015; Pentericci et al. 2016; Ferrara et al. 2019). Because our REBELS galaxies were selected via the Lyman break (Bouwens et al. 2022), they show Ly α EWs more typical of bright $z \sim 7$ systems and thus provide a valuable baseline for [C II] production in the reionization era. Below, we explore whether REBELS galaxies with higher Ly α EWs show significantly weaker [C II] emission at fixed SFR.

We divide our REBELS galaxies into two sub-samples split by Ly α EW = 10–20 Å and EW < 10 Å, where 10 Å is the approximate typical Ly α EW of UV-bright $z \sim 7$ galaxies (E21b). For this analysis, we ignore REBELS-03 and REBELS-27 given their relatively weak upper limits on Ly α EW from skyline contamination. The [C II] luminosities (Schouws et al., in preparation) and UV + IR star formation rates of each galaxy (Topping et al. 2022) are reported in Table 3.

Our current sample does not show a strong trend between Ly α EW and [C II] luminosity at fixed SFR. The three galaxies with relatively weak Ly α emission (EW < 10 Å) have [C II] luminosity to SFR ratios spanning $(0.06–0.13) \times 10^8 \, L_\odot/(M_\odot \, yr^{-1})$ with an average value of $(0.09 \pm 0.04) \times 10^8 \, L_\odot/(M_\odot \, yr^{-1})$. These $L_{[C II]}$/SFR ratios are very similar to the three more moderate Ly α emitters (EW = 10–20 Å) which show values spanning $(0.05–0.09) \times 10^8 \, L_\odot/(M_\odot \, yr^{-1})$ with an average of $(0.06 \pm 0.02) \times 10^8 \, L_\odot/(M_\odot \, yr^{-1})$. Here, we are adopting a fixed conversion factor between UV luminosity and unobscured SFR (see Section 2.2), as is common in the literature (e.g. Maiolino et al. 2015; Pentericci et al. 2016; Matthee et al. 2019). Utilizing age-dependent SFR_{UV}/L_{UV} ratios (e.g. Topping et al. 2022) does substantially increase the estimated unobscured SFRs of two sources (REBELS-15 and REBELS-39) given that their high [O III] + H β EWs suggest very young ages (see Section 2.2). However, since each Ly α EW bin contains one of these sources, we still find that the average $L_{[C II]}$/SFR ratios are comparable for weak and moderate Ly α emitters in our sample when adopting age-dependent SFR_{UV}/L_{UV} ratios.

There are two possible explanations for why we do not find significantly weaker [C II] emission (at fixed SFR) among the stronger Ly α emitters in our sample. The first potential reason is that our REBELS galaxies probe a rather limited dynamic range of Ly α EWs (<20 Å). Previous studies have found evidence that relatively weak [C II] production becomes more apparent among $z \gtrsim 6$ galaxies with Ly α EW $\gtrsim 50$ Å (e.g. Carniani et al. 2018a; Harikane et al. 2018b; Matthee et al. 2019). It is possible that only at such high EWs do galaxy properties which reduce [C II] production (e.g. low metallicity or strong stellar feedback; Ouchi et al. 2013; Vallini et al. 2015; Ferrara et al. 2019) become significantly more common. We also may not yet have adequate statistics to identify a modest correlation between $L_{[C II]}$/SFR ratios and Ly α emission at EW $\lesssim 20$ Å. Further rest-UV spectroscopic follow-up of the REBELS sample would better establish if a correlation is present in this typical Ly α EW regime.

5 DISCUSSION

Numerous observational campaigns have presented evidence that the IGM rapidly transitioned to a highly neutral state at $z > 6$ (e.g. Becker et al. 2001; Fan, Carilli & Keating 2006; Kashikawa et al. 2011;
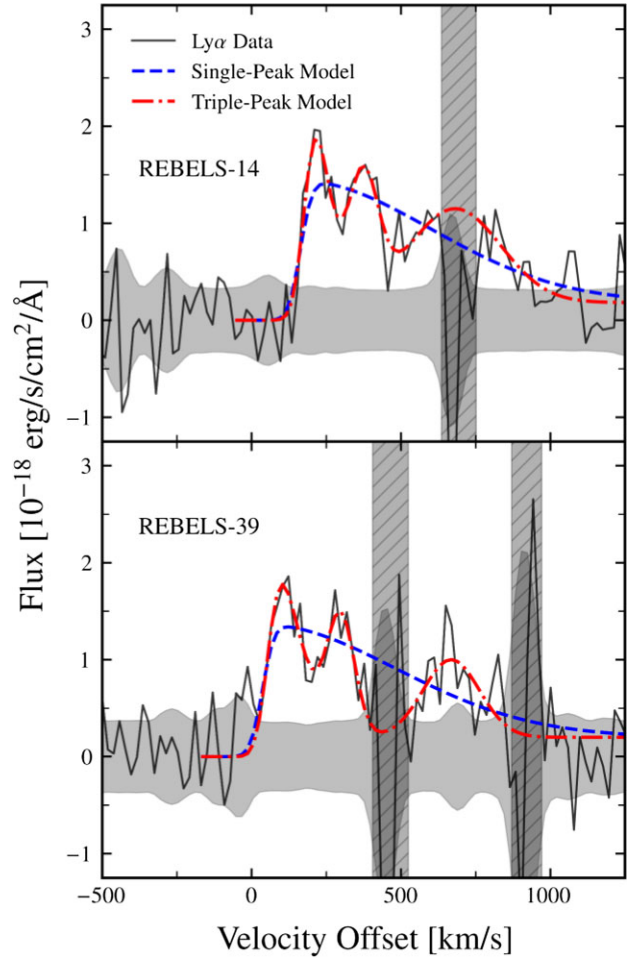

Figure 6. We find tentative evidence of multipeaked Ly α emission from REBELS-14 (top) and REBELS-39 (bottom). We show the MMT/Binospec data similar to Fig. 1 and overlay the best-fitting single-peak and triple-peak line profile models. Hashed grey regions show portions of the spectra overlapping with strong skylines that were not used in the fits. The triple-peak solutions provide a better match to the data (reduced $\chi^2 = 0.50–0.66$) compared to the single-peak solutions (reduced $\chi^2 = 1.16–1.20$) for both sources. These tentative multiple Ly α peaks (all redward of systemic) may be originating from multiple gas clumps moving with large peculiar motions within each galaxy.

Konno et al. 2014; McGreer et al. 2015; Greig et al. 2017; Zheng et al. 2017; Bañados et al. 2018; Davies et al. 2018; Wang et al. 2020; Whitler et al. 2020; Yang et al. 2020), thereby greatly increasing the optical depth to Ly α given its resonant nature. Surprisingly, UV-bright ($M_{UV} \lesssim -21$) galaxies show no evidence of strong evolution in Ly α emission strengths between $z \sim 6$ and $z \sim 7$ (Ono et al. 2012; Stark et al. 2017, E21b), raising the question of how photons from these systems were able to transmit efficiently through a partially neutral IGM. Using our ALMA observations, we have demonstrated that UV-bright $z \sim 7$ galaxies commonly exhibit both large Ly α velocity offsets and broad Ly α lines (Section 4). Here, we explore how these properties enhance Ly α transmission in the reionization era.

In this paper, we have nearly doubled the number of Ly α velocity offset measurements among extremely UV-luminous ($M_{UV} < -22$) Lyman-break galaxies at $z > 6$ (see Table 4). To quantify the expected IGM transmission of these systems, we calculate the damping wing optical depth (Miralda-Escudé 1998) faced by Ly α
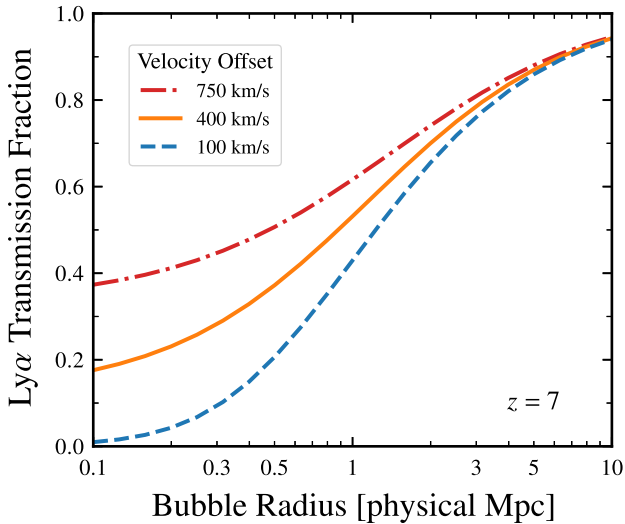
Figure 7. Illustration of how Ly α IGM damping wing transmission during reionization depends on both the bubble size and the Ly α photon velocity relative to systemic. We assume that the emitting galaxy is at $z = 7$ and resides in the centre of a highly ionized ($x_{\rm H\,I} \lesssim 10^{-5}$) bubble with radius in physical Mpc given by the x-axis. Extremely UV-luminous ($M_{\rm UV} < -22$) galaxies at $z > 6$ exhibit large velocity offsets (average $\approx 400\,{\rm km\,s^{-1}}$) and nearly half also show very broad profiles with detectable flux extending to $\sim 750\,{\rm km\,s^{-1}}$ (Fig. 4). At these high velocities, Ly α photons transmit efficiently ($\gtrsim 40$ per cent) through the neutral IGM even when emitted from within small ($R = 0.1$ physical Mpc) bubbles.

photons at their average velocity offset ($\approx 400\,{\rm km\,s^{-1}}$). We assume that the IGM outside the emitting galaxy is highly ionized ($x_{\rm H\,I} \lesssim 10^{-5}$) out to a bubble radius R beyond which the IGM is completely neutral. In a moderate-sized bubble ($R = 0.5$ physical Mpc), a typical extremely UV-luminous $z = 7$ galaxy will transmit a considerable fraction (≈ 35 per cent) of its Ly α emission at peak velocity ($\Delta{\rm v}_{\rm Ly\alpha} = 400\,{\rm km\,s^{-1}}$, see Fig. 7). Since the Ly α photons of these luminous systems are redshifted far past the resonant core, their IGM transmission will remain significant ($T \approx 20$ per cent) even if situated in small ($R = 0.1$ physical Mpc) bubbles.

Extremely UV-luminous ($M_{\rm UV} < -22$) $z > 6$ galaxies commonly exhibit not only large velocity offsets, but also broad Ly α profiles with an average FWHM $= 450\,{\rm km\,s^{-1}}$ (see Fig. 5a and Table 5). The combination of these two properties indicate that a substantial fraction of Ly α photons are frequently pushed deep into the damping wing where the H I absorption cross-section is minimized. Indeed, nearly half (3/7) of extremely UV-luminous $z > 6$ galaxies with Ly α detections and systemic redshift measurements show Ly α flux extending to $\approx 750\,{\rm km\,s^{-1}}$ (see Fig. 4 and Hashimoto et al. 2019), enabling Ly α photons transmit efficiently through the IGM even when emitted within a small ($R = 0.1$ physical Mpc) ionized bubble ($T \gtrsim 40$ per cent; see Fig. 7). This ability to displace Ly α photons to such high velocities clearly aids in the persistent visibility of massive, UV-luminous galaxies at $z > 6$.

With the Ly α velocity profile information of our Binospec-detected REBELS galaxies, we can estimate the net IGM transmission fraction for each system assuming a given ionized bubble size. That is, for each wavelength pixel in the observed 1D Ly α profiles (Fig. 1), we divide the line flux density by the IGM transmission fraction at the corresponding velocity and re-integrate the line profile to obtain an estimate of the line flux escaping from the interstellar and circumgalactic medium. For these UV-luminous

($-22.7 \leq M_{\rm UV} \leq -21.6$) $z \sim 7$ galaxies, we assume a fiducial bubble size of $R = 1$ physical Mpc (Endsley & Stark 2022) and estimate that approximately half (48–54 per cent) of the Ly α flux escaping from each galaxy has escaped through the IGM. If these highly UV-luminous systems are instead often situated in the centre of very large ($R \gtrsim 3$ physical Mpc) ionized bubbles (possibly as a result of surrounding strong galaxy overdensities; e.g. Barkana & Loeb 2004; Endsley & Stark 2022; Leonova et al. 2022), we then estimate that $\gtrsim 75$–80 per cent of their Ly α photons are transmitted through the IGM. Nevertheless, we expect that the high peak Ly α velocity offsets and large line widths of UV-luminous $z > 6$ galaxies lead to a relatively high net transmission ($\gtrsim 50$ per cent) of Ly α photons through the IGM.

In contrast to bright systems, faint ($-20 \lesssim M_{\rm UV} \lesssim -18$) galaxies show a strong decline in Ly α emission strengths at $z > 6$ (Schenker et al. 2014; Pentericci et al. 2018; Fuller et al. 2020). It is possible that this apparent luminosity dependence on Ly α transmission is (at least in part) due to smaller velocity offsets and narrower Ly α widths at lower UV luminosities. While such a picture is consistent with existing observations, all these measurements come from faint $z > 6$ sources with exceptionally strong Ly α emission (EW = 32–342 Å; see Tables 4 and 5) thereby potentially biasing this conclusion.

Until Ly α detections become more accessible for typical faint reionization-era galaxies, expectations of their IGM transmission properties must be guided by data at lower redshift. One particularly relevant result is that Ly α velocity offsets positively correlate with UV luminosity at $z \sim 2$–3 (Erb et al. 2014). Of course, if a similar relation holds at $z > 6$, the Ly α emission of fainter galaxies would be more susceptible to scattering by intergalactic H I. To better quantify the possible extent of this effect, Mason et al. (2018a) developed a model calibrated to the $z \sim 2 - 3$ data that predicts a galaxy's velocity offset given its UV luminosity and redshift. The main assumption underlying this model is that velocity offsets correlate with halo mass independently of redshift, and can therefore be linked to UV luminosity via theoretical $M_{\rm UV}$–$M_{\rm halo}$ relations. With our results, we can begin testing this model's predictions at $z \sim 7$. From the seven extremely UV-luminous ($-23 < M_{\rm UV} < -22$) Lyman-break galaxies at $z = 6 - 8$ with robust velocity offset measurements, we calculate an average of $\langle \Delta{\rm v}_{\rm Ly\alpha} \rangle = 387\,{\rm km\,s^{-1}}$ (Table 4). The Mason et al. (2018a) model predicts this empirical value within ≈ 0.1 dex ($\langle \Delta{\rm v}_{\rm Ly\alpha} \rangle \approx 300\,{\rm km\,s^{-1}}$ for $M_{\rm UV} = -22.5$ and $z = 7$), indicating reasonable agreement (see Fig. 3). Assuming this model can be applied to lower luminosities, we would expect a typical faint ($M_{\rm UV} = -19$) galaxy at $z = 7$ to show a velocity offset of $\approx 100\,{\rm km\,s^{-1}}$ which is consistent with measurements from A383-5.2 ($z = 6.03$, $M_{\rm UV} = -19.3$; Stark et al. 2015; Knudsen et al. 2016). The Ly α IGM transmission at this velocity offset is nearly half that at $\Delta{\rm v}_{\rm Ly\alpha} = 400\,{\rm km\,s^{-1}}$ assuming a moderate-sized ($R = 0.5$ physical Mpc) host bubble at $z = 7$ (see Fig. 7). The difference becomes much more substantial in smaller bubbles ($R = 0.1$ physical Mpc) where Ly α transmission is only $T \approx 1$ per cent at $100\,{\rm km\,s^{-1}}$ compared with $T \approx 20$ per cent at $400\,{\rm km\,s^{-1}}$.

Another relevant question is how we might expect Ly α FWHM to vary with UV luminosity in the reionization era. Data at lower redshift again provides a valuable baseline. Upon investigating a large set of literature Ly α observations (primarily at $z \sim 0 - 4$), Verhamme et al. (2018) found a positive correlation between the FWHM and the velocity offset of the red Ly α peak. This observed trend may arise in part from larger H I column densities both broadening the Ly α line as well as pushing the peak of emission to higher velocities (e.g. Verhamme et al. 2006, 2018; Zheng et al. 2014). Outflows may also help drive this correlation since systems with gas extending to higher

velocities would be expected to show both a wider Ly α profile and a more redshifted peak. If fainter $z > 6$ galaxies have systematically lower H I column densities or slower outflows (perhaps due to lower mass), they would, thus, be expected to show narrower Ly α lines in addition to smaller velocity offsets. While the lower H I column densities may lead to more efficient Ly α escape within the galaxy, the resulting narrower and less redshifted lines will face stronger attenuation from the partially neutral $z \gtrsim 7$ IGM. Assuming an average velocity offset of $\approx 100 \, \text{km s}^{-1}$ for faint ($M_{\text{UV}} \sim -19$) galaxies at $z = 7$ (Mason et al. 2018a), the literature compilation from Verhamme et al. (2018) suggests a typical FWHM of $\approx 200–250 \, \text{km s}^{-1}$. This is consistent with measurements from RELICS-DP7, A838-5.2, and MACS0744-064 ($-19.5 \leq M_{\text{UV}} \leq -18.5$) which show an average FWHM = $190 \, \text{km s}^{-1}$ (Stark et al. 2015; Hoag et al. 2019; Pelliccia et al. 2021), and implies that the Ly α flux from faint $z = 7$ galaxies would often be limited to $\lesssim 300 \, \text{km s}^{-1}$ relative to systemic. At these velocities, IGM transmission will be considerably suppressed (factor > 3) in small ($R \sim 0.1$ physical Mpc) bubbles relative to the UV-bright systems that have emission extending to $\approx 750 \, \text{km s}^{-1}$.

These predictions help explain why it has been so challenging to detect Ly α emission from faint $z \gtrsim 7$ galaxies, even those which appear to sit in the vicinity of an ionized bubble. One likely ionized region is in the BDF field where three relatively bright ($M_{\text{UV}} \leq -20.5$) galaxies at $z = 7.0–7.1$ exhibit strong Ly α emission (Vanzella et al. 2011; Castellano et al. 2018). However, deep follow-up observations yielded no Ly α detections among all twelve fainter ($M_{\text{UV}} > -20.25$) $z \sim 7$ candidates targeted in this field (Castellano et al. 2018). While it is currently unclear whether these faint systems indeed reside in the same ionized structure(s), it is none the less expected that their Ly α photons would experience weaker IGM transmission due to smaller velocity offsets and narrower line widths. Using the predictions described above, an intrinsically faint ($M_{\text{UV}} \sim -19$) $z = 7$ galaxy would likely have $\approx 2 \times$ lower Ly α IGM transmission relative to an extremely luminous ($M_{\text{UV}} < -22$) system assuming a moderate-sized ($R = 0.5$ physical Mpc) host bubble. These expectations for reduced IGM transmission also help explain the dearth of Ly α detections among faint yet lensed $z \sim 7–8$ galaxies (Hoag et al. 2019; Mason et al. 2019).

6 SUMMARY

We present MMT/Binospec Ly α spectra of eight UV-luminous ($-22.7 \leq M_{\text{UV}} \leq -21.6$), massive ($8.7 \leq \log (M_*/M_\odot) \leq 9.5$) [C II]-detected galaxies at $z = 6.5–7.1$ selected from the recent ALMA Large program REBELS (Bouwens et al. 2022). With this data, we report four new measurements of Ly α velocity offsets among UV-bright reionization-era galaxies, improving our understanding of how their photons transmit efficiently through a partially neutral IGM. We also investigate the role played by the broad Ly α profiles of UV-luminous $z > 6$ galaxies. Our conclusions are as follows:

(i) We confidently ($> 7\sigma$) detect Ly α in four of eight [C II]-detected REBELS galaxies that we have so far targeted with MMT/Binospec. The Ly α EWs of our detected sources range between 3.7 and 14.6 Å which are all typical of massive UV-luminous $z \simeq 7$ galaxies (E21b). For two of the sources lacking a Ly α detection, we place stringent 5σ EW limits of ≤ 6 Å given the lack of skylines in the relevant part of the spectrum.

(ii) Among the four REBELS galaxies with Binospec detections, we measure Ly α velocity offsets of 165, 177, 227, and 324 km s^{-1}.

Our sample nearly doubles the number of velocity offset measurements among extremely UV-luminous ($M_{\text{UV}} < -22$) Lyman-break selected galaxies at $z > 6$. All seven of these systems show large ($> 100 \, \text{km s}^{-1}$) velocity offsets, indicating that their Ly α photons are pushed well past the strong resonant core of the H I absorption cross-section. At their average velocity offset of $387 \, \text{km s}^{-1}$, Ly α photons transmit efficiently through the IGM with $T \approx 35$ per cent when emerging from a $z = 7$ galaxy situated in a moderate-sized ($R = 0.5$ physical Mpc), highly ionized ($x_{\text{H I}} < 10^{-5}$) bubble.

(iii) All four REBELS galaxies with Binospec detections display broad Ly α lines with FWHM $> 300 \, \text{km s}^{-1}$, indicating that a large fraction of their photons are at high velocities where damping wing absorption is weaker. Two of these galaxies show extremely broad Ly α profiles (FWHM = $640 \, \text{km s}^{-1}$) with significant emission extending to $\approx 750 \, \text{km s}^{-1}$ relative to systemic. At such high velocities, Ly α photons transmit efficiently ($T \gtrsim 40$ per cent) through the IGM, even when the emitting source resides in a small ($R = 0.1$ physical Mpc) ionized bubble. Broad Ly α profiles (FWHM = $300–400 \, \text{km s}^{-1}$) are also observed from the three other UV-luminous ($M_{\text{UV}} < -22$) continuum-selected $z > 6$ galaxies in the literature (Cuby et al. 2003; Willott et al. 2013; Oesch et al. 2015), indicating an average FWHM = $450 \, \text{km s}^{-1}$ for this population. These broad line widths undoubtedly assist in boosting the Ly α visibility of UV-bright galaxies at $z \gtrsim 7$.

(iv) A contributing factor to the broad Ly α profiles of massive, UV-bright $z > 6$ galaxies may be that their Ly α emission is produced in gas spanning a wide range of motions, as evidenced by our ALMA data. In the two REBELS galaxies showing extremely broad Ly α profiles, we also observe very broad [C II] emission (FWHM = $300–520 \, \text{km s}^{-1}$) indicating that these are composite galaxies containing multiple gas clumps moving with large peculiar motions (e.g. Bowler et al. 2017; Carniani et al. 2018a). If these high-velocity gas clumps also produce Ly α emission, the intrinsic Ly α profile will mirror that of [C II] before being further broadened by resonant interactions with outflowing material. The large peculiar motions of these clumps might also produce Ly α profiles with multiple peaks redward of systemic velocity. Such profiles are different in nature from those showing a peak blueward of systemic which signal low H I column density channels on the near side of the galaxy (e.g. Gazagnes et al. 2020). We suggest that systemic redshifts from [C II] and other non-resonant lines are critical to interpret the physical origin of multipeaked Ly α lines.

(v) We find no strong trend between the strength of Ly α emission and the [C II] luminosity at fixed SFR in our REBELS sample. The three galaxies with relatively weak Ly α emission (EW < 10 Å) show an average [C II] luminosity to SFR ratio that is very similar to the average ratio among the three more moderate Ly α emitters (EW = $10–20$ Å). This lack of an apparent trend may be due to the limited dynamic range in Ly α EWs among our Lyman-break selected sample, though improved statistics are also required to test for a modest correlation in this EW regime.

(vi) Recent studies may suggest that faint galaxies in the vicinity of ionized bubbles at $z \sim 7$ do not show strong Ly α emission (Castellano et al. 2018). While this could imply relatively small bubbles around bright sources, it may also reflect a luminosity dependence on the Ly α profile properties discussed in this paper. Faint ($M_{\text{UV}} \sim -19$) $z \sim 7$ galaxies are expected to typically exhibit much smaller velocity offsets ($\Delta v_{\text{Ly}\alpha} \sim 100 \, \text{km s}^{-1}$; Mason et al. 2018a) and narrower line widths (FWHM$\sim 200–250 \, \text{km s}^{-1}$; Verhamme et al. 2018) relative to that seen among extremely luminous ($M_{\text{UV}} < -22$) systems. These predictions imply $\approx 2 \times$ lower IGM transmission among faint $z = 7$ galaxies at fixed moderate bubble size of $R = 0.5$

physical Mpc, helping explain why their emission is more difficult to detect.

DATA AVAILABILITY

The near- and mid-infrared imaging data underlying this article are available through their respective data repositories. See http://www.eso.org/rm/publicAccess#/dataReleases for UltraVISTA and VIDEO data, and https://sha.ipac.caltech.edu/applications/Spitzer/SHA/ for IRAC data. The raw ALMA data are available via the science archive (program 2019.1.01634.L) and the MMT/Binospec data will be shared upon reasonable request to the corresponding author.

REFERENCES

Astropy Collaboration, 2013, A&A, 558, A33
Bañados E. et al., 2018, Nature, 553, 473
Barkana R., Loeb A., 2004, ApJ, 609, 474
Barone-Nugent R. L. et al., 2014, ApJ, 793, 17
Becker R. H. et al., 2001, AJ, 122, 2850
Behrens C., Pallottini A., Ferrara A., Gallerani S., Vallini L., 2019, MNRAS, 486, 2197
Béthermin M. et al., 2015, A&A, 573, A113
Béthermin M. et al., 2020, A&A, 643, A2
Bouwens R. J. et al., 2014, ApJ, 793, 115
Bouwens R. J. et al., 2022, ApJ, 931, 160
Bowler R. A. A. et al., 2014, MNRAS, 440, 2810
Bowler R. A. A., Dunlop J. S., McLure R. J., McLeod D. J., 2017, MNRAS, 466, 3612
Bowler R. A. A., Jarvis M. J., Dunlop J. S., McLure R. J., McLeod D. J., Adams N. J., Milvang-Jensen B., McCracken H. J., 2020, MNRAS, 493, 2059
Bowler R. A. A., Cullen F., McLure R. J., Dunlop J. S., Avison A., 2022, MNRAS, 510, 5088
Bruzual G., Charlot S., 2003, MNRAS, 344, 1000
Carniani S. et al., 2017, A&A, 605, A42
Carniani S. et al., 2018a, MNRAS, 478, 1170
Carniani S., Maiolino R., Smit R., Amorín R., 2018b, ApJ, 854, L7
Carniani S. et al., 2020, MNRAS, 499, 5136
Caruana J., Bunker A. J., Wilkins S. M., Stanway E. R., Lorenzoni S., Jarvis M. J., Ebert H., 2014, MNRAS, 443, 2831
Cassata P. et al., 2015, A&A, 573, A24
Cassata P. et al., 2020, A&A, 643, A6
Castellano M. et al., 2016, ApJ, 818, L3
Castellano M. et al., 2017, ApJ, 839, 73
Castellano M. et al., 2018, ApJ, 863, L3
Chabrier G., 2003, PASP, 115, 763
Chevallard J., Charlot S., 2016, MNRAS, 462, 1415
Chevallard J. et al., 2018, MNRAS, 479, 3264
Ciardullo R. et al., 2014, ApJ, 796, 64
Claeyssens A. et al., 2019, MNRAS, 489, 5022
Cuby J. G., Le Fèvre O., McCracken H., Cuillandre J. C., Magnier E., Meneux B., 2003, A&A, 405, L19
Curtis-Lake E. et al., 2016, MNRAS, 457, 440
Davies F. B. et al., 2018, ApJ, 864, 142
Dayal P., Ferrara A., 2018, Phys. Rep., 780, 1
Dayal P., Ferrara A., Saro A., Salvaterra R., Borgani S., Tornatore L., 2009, MNRAS, 400, 2000
Dayal P. et al., 2022, MNRAS, 512, 989
De Barros S. et al., 2017, A&A, 608, A123
De Barros S., Oesch P. A., Labbé I., Stefanon M., González V., Smit R., Bouwens R. J., Illingworth G. D., 2019, MNRAS, 489, 2355
De Looze I. et al., 2014, A&A, 568, A62
Dijkstra M., 2014, PASA, 31, e040
Dijkstra M., 2017, preprint (arXiv:1704.03416)
Emami N., Siana B., Alavi A., Gburek T., Freeman W. R., Richard J., Weisz D. R., Stark D. P., 2020, ApJ, 895, 116
Endsley R., Stark D. P., 2022, MNRAS, 511, 6042
Endsley R., Stark D. P., Chevallard J., Charlot S., 2021a, MNRAS, 500, 5229
Endsley R., Stark D. P., Charlot S., Chevallard J., Robertson B., Bouwens R. J., Stefanon M., 2021b, MNRAS, 502, 6044 (E21b)

Erb D. K. et al., 2014, ApJ, 795, 33
Erb D. K., Steidel C. C., Chen Y., 2018, ApJ, 862, L10
Fabricant D. et al., 2019, PASP, 131, 075004
Faisst A. L. et al., 2020, ApJS, 247, 61
Fan X., Carilli C. L., Keating B., 2006, ARA&A, 44, 415
Ferland G. J. et al., 2013, RMxAA, 49, 137
Feroz F., Hobson M. P., 2008, MNRAS, 384, 449
Feroz F., Hobson M. P., Bridges M., 2009, MNRAS, 398, 1601
Ferrara A., Vallini L., Pallottini A., Gallerani S., Carniani S., Kohandel M., Decataldo D., Behrens C., 2019, MNRAS, 489, 1
Ferrara A. et al., 2022, MNRAS, 512, 58
Fontana A. et al., 2010, ApJ, 725, L205
Fudamoto Y. et al., 2021, Nature, 597, 489
Fuller S. et al., 2020, ApJ, 896, 156
Furusawa H. et al., 2016, ApJ, 822, 46
Garaldi E., Kannan R., Smith A., Springel V., Pakmor R., Vogelsberger M., Hernquist L., 2022, MNRAS, 512, 4909
Gazagnes S., Chisholm J., Schaerer D., Verhamme A., Izotov Y., 2020, A&A, 639, A85
Greig B., Mesinger A., Haiman Z., Simcoe R. A., 2017, MNRAS, 466, 4239
Gutkin J., Charlot S., Bruzual G., 2016, MNRAS, 462, 1757
Harikane Y. et al., 2018a, PASJ, 70, S11
Harikane Y. et al., 2018b, ApJ, 859, 84
Hashimoto T., Ouchi M., Shimasaku K., Ono Y., Nakajima K., Rauch M., Lee J., Okamura S., 2013, ApJ, 765, 70
Hashimoto T. et al., 2019, PASJ, 71, 71
Hayes M. et al., 2010, Nature, 464, 562
Hayes M. J., Runnholm A., Gronke M., Scarlata C., 2021, ApJ, 908, 36
Henry A., Scarlata C., Martin C. L., Erb D., 2015, ApJ, 809, 19
Hoag A. et al., 2019, ApJ, 878, 12
Horne K., 1986, PASP, 98, 609
Hu E. M., Cowie L. L., Barger A. J., Capak P., Kakazu Y., Trouille L., 2010, ApJ, 725, 394
Hu W. et al., 2019, ApJ, 886, 90
Hu W. et al., 2021, Nature Astron., 5, 485
Hunter J. D., 2007, Comput. Sci. Engineer., 9, 90
Hutter A., Dayal P., Müller V., Trott C. M., 2017, ApJ, 836, 176
Inami H. et al., 2022, MNRAS, 515, 3126
Itoh R. et al., 2018, ApJ, 867, 46
Jaskot A. E., Dowd T., Oey M. S., Scarlata C., McKinney J., 2019, ApJ, 885, 96
Jones E. et al., 2001, SciPy: Open Source Scientific Tools for Python. Available at http://www.scipy.org/
Jones G. C., Willott C. J., Carilli C. L., Ferrara A., Wang R., Wagg J., 2017, ApJ, 845, 175
Jung I. et al., 2017, ApJ, 834, 81
Jung I. et al., 2020, ApJ, 904, 144
Kannan R., Garaldi E., Smith A., Pakmor R., Springel V., Vogelsberger M., Hernquist L., 2022, MNRAS, 511, 4005
Kansky J. et al., 2019, PASP, 131, 075005
Kashikawa N. et al., 2011, ApJ, 734, 119
Kennicutt, Robert C. J., 1998, ARA&A, 36, 189
Knudsen K. K., Richard J., Kneib J.-P., Jauzac M., Clément B., Drouart G., Egami E., Lindroos L., 2016, MNRAS, 462, L6
Kohandel M., Pallottini A., Ferrara A., Zanella A., Behrens C., Carniani S., Gallerani S., Vallini L., 2019, MNRAS, 487, 3007
Kohandel M., Pallottini A., Ferrara A., Carniani S., Gallerani S., Vallini L., Zanella A., Behrens C., 2020, MNRAS, 499, 1250
Konno A. et al., 2014, ApJ, 797, 16
Konno A. et al., 2018, PASJ, 70, S16
Kriek M. et al., 2015, ApJS, 218, 15
Labbé I. et al., 2013, ApJ, 777, L19
Laporte N., Nakajima K., Ellis R. S., Zitrin A., Stark D. P., Mainali R., Roberts-Borsani G. W., 2017, ApJ, 851, 40
Le Fèvre O. et al., 2020, A&A, 643, A1
Leclercq F. et al., 2020, A&A, 635, A82
Leonova E. et al., 2022, MNRAS, 515, 5790
McGreer I. D., Mesinger A., D'Odorico V., 2015, MNRAS, 447, 499

Mainali R., Kollmeier J. A., Stark D. P., Simcoe R. A., Walth G., Newman A. B., Miller D. R., 2017, ApJ, 836, L14
Maiolino R. et al., 2015, MNRAS, 452, 54
Mas-Hesse J. M., Kunth D., Tenorio-Tagle G., Leitherer C., Terlevich R. J., Terlevich E., 2003, ApJ, 598, 858
Mason C. A., Gronke M., 2020, MNRAS, 499, 1395
Mason C. A., Treu T., Dijkstra M., Mesinger A., Trenti M., Pentericci L., de Barros S., Vanzella E., 2018a, ApJ, 856, 2
Mason C. A. et al., 2018b, ApJ, 857, L11
Mason C. A. et al., 2019, MNRAS, 485, 3947
Matthee J., Sobral D., Oteo I., Best P., Smail I., Röttgering H., Paulino-Afonso A., 2016, MNRAS, 458, 449
Matthee J. et al., 2017, ApJ, 851, 145
Matthee J., Sobral D., Gronke M., Paulino-Afonso A., Stefanon M., Röttgering H., 2018, A&A, 619, A136
Matthee J. et al., 2019, ApJ, 881, 124
Matthee J., Sobral D., Gronke M., Pezzulli G., Cantalupo S., Röttgering H., Darvish B., Santos S., 2020, MNRAS, 492, 1778
Mesinger A., Haiman Z., Cen R., 2004, ApJ, 613, 23
Meyer R. A., Laporte N., Ellis R. S., Verhamme A., Garel T., 2021, MNRAS, 500, 558
Miralda-Escudé J., 1998, ApJ, 501, 15
Mortlock D. J. et al., 2011, Nature, 474, 616
Nagao T. et al., 2005, ApJ, 634, 142
Neufeld D. A., 1990, ApJ, 350, 216
Oesch P. A. et al., 2015, ApJ, 804, L30
Ono Y. et al., 2012, ApJ, 744, 83
Osterbrock D. E., Ferland G. J., 2006, Astrophysics of Gaseous Nebulae and Active Galactic Nuclei, 2nd edn. University Science Books, Sausalito
Ota K. et al., 2014, ApJ, 792, 34
Ota K. et al., 2017, ApJ, 844, 85
Ouchi M. et al., 2010, ApJ, 723, 869
Ouchi M. et al., 2013, ApJ, 778, 102
Ouchi M., Ono Y., Shibuya T., 2020, ARA&A, 58, 617
Pallottini A. et al., 2019, MNRAS, 487, 1689
Park H. et al., 2021, ApJ, 922, 263
Pei Y. C., 1992, ApJ, 395, 130
Pelliccia D. et al., 2021, ApJ, 908, L30
Pentericci L. et al., 2011, ApJ, 743, 132
Pentericci L. et al., 2014, ApJ, 793, 113
Pentericci L. et al., 2016, ApJ, 829, L11
Pentericci L. et al., 2018, A&A, 619, A147
Planck Collaboration VI, 2020, A&A, 641, A6
Price-Whelan A. M. et al., 2018, AJ, 156, 123
Qin Y., Wyithe J. S. B., Oesch P. A., Illingworth G. D., Leonova E., Mutch S. J., Naidu R. P., 2022, MNRAS, 510, 3858
Robertson B. E., 2022, ARA&A, 60, 121
Salmon B. et al., 2015, ApJ, 799, 183
Schaerer D., de Barros S., 2010, A&A, 515, A73
Schaerer D., Boone F., Zamojski M., Staguhn J., Dessauges-Zavadsky M., Finkelstein S., Combes F., 2015, A&A, 574, A19
Schenker M. A., Ellis R. S., Konidaris N. P., Stark D. P., 2014, ApJ, 795, 20
Schouws S. et al., 2022, ApJ, 928, 31
Shapley A. E., Steidel C. C., Pettini M., Adelberger K. L., 2003, ApJ, 588, 65
Shibuya T. et al., 2014, ApJ, 788, 74
Smit R. et al., 2014, ApJ, 784, 58
Smith A., Kannan R., Garaldi E., Vogelsberger M., Pakmor R., Springel V., Hernquist L., 2022, MNRAS, 512, 3243
Sobral D., Matthee J., Darvish B., Schaerer D., Mobasher B., Röttgering H. J. A., Santos S., Hemmati S., 2015, ApJ, 808, 139
Sommovigo L. et al., 2022, MNRAS, 513, 3122
Stark D. P., Ellis R. S., Chiu K., Ouchi M., Bunker A., 2010, MNRAS, 408, 1628
Stark D. P., Ellis R. S., Ouchi M., 2011, ApJ, 728, L2
Stark D. P., Schenker M. A., Ellis R., Robertson B., McLure R., Dunlop J., 2013, ApJ, 763, 129
Stark D. P. et al., 2015, MNRAS, 450, 1846

Stark D. P. et al., 2017, MNRAS, 464, 469

Stefanon M. et al., 2017, ApJ, 851, 43

Stefanon M. et al., 2019, ApJ, 883, 99

Stefanon M., Bouwens R. J., Labbé I., Illingworth G. D., Oesch P. A., van Dokkum P., Gonzalez V., 2022, ApJ, 927, 48

Steidel C. C., Erb D. K., Shapley A. E., Pettini M., Reddy N., Bogosavljević M., Rudie G. C., Rakic O., 2010, ApJ, 717, 289

Steidel C. C., Bogosavljević M., Shapley A. E., Kollmeier J. A., Reddy N. A., Erb D. K., Pettini M., 2011, ApJ, 736, 160

Steidel C. C., Strom A. L., Pettini M., Rudie G. C., Reddy N. A., Trainor R. F., 2016, ApJ, 826, 159

Strait V. et al., 2020, ApJ, 888, 124

Tang M., Stark D. P., Chevallard J., Charlot S., 2019, MNRAS, 489, 2572

Tilvi V. et al., 2020, ApJ, 891, L10

Topping M. W. et al., 2022, MNRAS, 516, 975

Vallini L., Gallerani S., Ferrara A., Pallottini A., Yue B., 2015, ApJ, 813, 36

Van Der Walt S., Colbert S. C., Varoquaux G., 2011, Comput. Sci. Engineer., 13, 22

Vanzella E. et al., 2011, ApJ, 730, L35

Vanzella E. et al., 2014, ApJ, 783, L12

Verhamme A., Schaerer D., Maselli A., 2006, A&A, 460, 397

Verhamme A., Schaerer D., Atek H., Tapken C., 2008, A&A, 491, 89

Verhamme A., Orlitová I., Schaerer D., Hayes M., 2015, A&A, 578, A7

Verhamme A. et al., 2018, MNRAS, 478, L60

Wang F. et al., 2020, ApJ, 896, 23

Weinberger L. H., Kulkarni G., Haehnelt M. G., Choudhury T. R., Puchwein E., 2018, MNRAS, 479, 2564

Weiss L. H. et al., 2021, ApJ, 912, 100

Whitler L. R., Mason C. A., Ren K., Dijkstra M., Mesinger A., Pentericci L., Trenti M., Treu T., 2020, MNRAS, 495, 3602

Willott C. J. et al., 2013, AJ, 145, 4

Willott C. J., Carilli C. L., Wagg J., Wang R., 2015, ApJ, 807, 180

Wold I. G. B. et al., 2022, ApJ, 927, 36

Wyithe J. S. B., Loeb A., 2005, ApJ, 625, 1

Yang J. et al., 2020, ApJ, 897, L14

Zheng Z.-Y., Wang J.-X., Malhotra S., Rhoads J. E., Finkelstein S. L., Finkelstein K., 2014, MNRAS, 439, 1101

Zheng Z.-Y. et al., 2017, ApJ, 842, L22

Zitrin A. et al., 2015, ApJ, 810, L12

[1] *Steward Observatory, University of Arizona, 933 N Cherry Ave, Tucson, AZ 85721, USA*

[2] *Leiden Observatory, Leiden University, NL-2300 RA Leiden, the Netherlands*

[3] *Astrophysics Research Institute, Liverpool John Moores University, 146 Brownlow Hill, Liverpool L3 5RF, UK*

[4] *Hiroshima Astrophysical Science Center, Hiroshima University, 1-3-1 Kagamiyama, Higashi-Hiroshima, Hiroshima 739-8526, Japan*

[5] *Astrophysics, The Denys Wilkinson Building, University of Oxford, Keble Road, Oxford OX1 3RH, UK*

[6] *Jodrell Bank Centre for Astrophysics, Department of Physics and Astronomy, School of Natural Sciences, The University of Manchester, Manchester M13 9PL, UK*

[7] *Observatoire de Genéve, CH-1290 Versoix, Switzerland*

[8] *Cosmic Dawn Center (DAWN), Niels Bohr Institute, University of Copenhagen, Jagtvej 128, DK-2200 København N, Denmark*

[9] *Departmento de Astronomia, Universidad de Chile, Casilla 36-D, Santiago 7591245, Chile*

[10] *Centro de Astrofisica y Tecnologias Afines (CATA), Camino del Observatorio 1515, Las Condes, Santiago 7591245, Chile*

[11] *Nucleo de Astronomia, Facultad de Ingenieria y Ciencias, Universidad Diego Portales, Av. Ejercito 441, Santiago 8370191, Chile*

[12] *International Centre for Radio Astronomy Research, University of Western Australia, 35 Stirling Hwy., Crawley, WA 6009, Australia*

[13] *Kapteyn Astronomical Institute, University of Groningen, PO Box 800, NL-9700 AV Groningen, the Netherlands*

[14] *Scuola Normale Superiore, Piazza dei Cavalieri 7, I-50126 Pisa, Italy*

[15] *Dipartimento di Fisica, Sapienza, Universita di Roma, Piazzale Aldo Moro 5, I-00185 Roma, Italy*

[16] *INAF/Osservatorio Astrofisico di Arcetri, Largo E. Femi 5, I-50125 Firenze, Italy*

[17] *Centre for Astrophysics and Supercomputing, Swinburne University of Technology, PO Box 218, Hawthorn, VIC 3112, Australia*

[18] *INAF/Osservatorio Astronomico di Roma, via Frascati 33, Monte Porzio Catone, I-00078 Roma, Italy*

[19] *Sapienza School for Advanced Studies, Sapienza Università di Roma, P.le Aldo Moro 2, I-00185 Roma, Italy*

[20] *INFN, Sezione di Roma 1, P.le Aldo Moro 2, I-00185 Roma, Italy*

This paper has been typeset from a TEX/LATEX file prepared by the author.